Département de physique
Université de Fribourg (Suisse)

Atomic level widths and shake probabilities as inferred from high-resolution measurements of x-ray emission spectra

THESE

présentée à la Faculté des Sciences de l'Université de Fribourg (Suisse)
pour l'obtention du grade de *Doctor rerum naturalium*

Pierre-Alexandre Raboud
de Villarsiviriaux (FR)

Thèse No 1362

Edition privée
2001

Acceptée par la Faculté des Sciences de l'Université de Fribourg (Suisse) sur proposition de:

Prof. Dr. J.-Cl. Dousse, Université de Fribourg, Directeur de Thèse,
Prof. Dr. A. Weis, Université de Fribourg, Rapporteur,
Prof. Dr. J. L. Campbell, University of Guelph Canada, Rapporteur.

Fribourg, le 12 décembre 2001

Le Directeur de thèse:

Prof. Dr. J.-Cl. Dousse

Le Doyen

Prof. Dr. A. von Zelewsky

Table des matières

Résumé

Ce travail de doctorat comprend deux volets appartenant tous deux au domaine de la physique atomique. Le premier concerne la largeur naturelle des couches et sous-couches profondes de l'atome. Le second est une étude des mécanismes conduisant à la création d'états atomiques *KL* doublement excités dans une cible gazeuse d'argon irradiée par des photons monoénergétiques.

Le premier projet contient lui-même deux parties : la première est une étude expérimentale des largeurs naturelles des sous-couches L_1 ($2s_{1/2}$) à N_5 ($4d_{5/2}$) de deux éléments lourds, l'uranium et le thorium. La seconde partie est une étude similaire portant cependant exclusivement sur la largeur de la sous-couche L_1 de divers éléments compris entre le samarium ($Z = 62$) et le bismuth ($Z = 83$). Dans les deux parties de ce projet, l'obtention de résultats fiables ne pouvait être obtenue qu'avec un instrument ayant un pouvoir de résolution comparable aux largeurs naturelles étudiées, c'est-à-dire de l'ordre de l'électron-volt pour un domaine d'énergie compris entre 2 et 20 keV. Cette condition restreignait le choix des instruments de mesure aux spectromètres à cristal.

Dans le second projet, la méthode expérimentale utilisée a consisté à comparer les énergies et intensités des transitions radiatives $1s^12s^22p^5 \rightarrow 1s^22s^22p^4$ et $1s^12s^12p^6 \rightarrow 1s^22s^12p^5$ à celles de la transition $1s^12s^22p^6 \rightarrow 1s^22s^22p^5$. A cause de la lacune spectatrice $2s$ ou $2p$, les raies X satellites $K\alpha_{1,2}L^{(1)}$ associées aux deux premières transitions sont déplacées vers les hautes énergies par rapport aux raies X diagrammes $K\alpha_{1,2}L^{(0)}$ associées à la troisième transition. A partir de l'intensité relative des raies satellites et diagrammes, la probabilité d'excitation double peut être déduite, ceci à condition de pouvoir résoudre les deux groupes de lignes spectrales. Comme la différence d'énergie n'est que d'environ 20 eV dans le cas de l'argon, là aussi le recours au spectromètre à cristal s'est avéré indispensable.

La spectroscopie de rayons X de haute-résolution représente donc le dénominateur commun des deux projets constituant cette thèse de doctorat. Des informations plus détaillées sur chacun des projets sont données ci-dessous.

Largeurs naturelles des niveaux atomiques

Des données précises et fiables concernant les largeurs naturelles des niveaux atomiques sont d'intérêt aussi bien pour la physique théorique qu'expérimentale. En physique théorique, de telles données permettent d'apprécier la précision des prédictions concernant la durée de vie moyenne d'une lacune, les probabilités de transition radiative ou Auger, ou encore les rapports de fluorescence. En physique expérimentale, une bonne connaissance de la forme des lignes spectrales est primordiale dans les méthodes d'analyse (XRF, PIXE) basées sur la mesure des rayons X de fluorescence émis par l'échantillon car elle permet d'augmenter la sensibilité et la précision de la méthode. En spectroscopie X de haute-résolution, de telles données sont aussi très utiles surtout lorsqu'il s'agit de résoudre des

structures de faible intensité (rayons X satellites, raies provenant de l'émission radiative-Auger) apparaissant à proximité de lignes spectrales beaucoup plus intenses. Dans ce cas la connaissance précise des largeurs naturelles permet de fixer la forme des raies de forte intensité et de diminuer ainsi le nombre de paramètres libres dans l'analyse du spectre.

Il existe très peu de données précises pour la largeur naturelle des transitions L d'éléments lourds car les énergies de ces transitions sont comprises dans un domaine peu favorable à leur mesure par des spectromètres à cristal. En général, les spectromètres à cristal de type transmission ne permettent pas en effet l'observation de photons de moins de 20 keV alors que les spectromètres de type réflexion sont rarement opérationnels au-dessus de 8-10 keV. Le spectromètre à cristal courbé DuMond de transmission de Fribourg permet toutefois la mesure de rayons X jusqu'à une énergie minimale d'environ 11 keV. Ceci a été rendu possible grâce à l'emploi de lames cristallines de faible épaisseur (0.5 mm) et au domaine angulaire exceptionnellement grand (± 20 degrés) que cet instrument permet de couvrir. Mettant à profit ces propriétés, nous avons mesuré plus de 30 transitions L du thorium. Les énergies et largeurs naturelles de ces transitions ont pu être déterminées avec une très bonne précision. Comme la largeur d'une transition est égale à la somme des largeurs des deux niveaux atomiques impliqués dans cette transition, il est possible, sous certaines conditions, de déterminer la largeur des niveaux à partir des largeurs des transitions mesurées. Dans le cas du thorium, la méthode ne s'est avérée possible que par l'adjonction de quelques transitions M. Celles-ci, au nombre de 10, ont été mesurées au moyen d'un spectromètre à cristal von Hamos de réflexion. A partir des largeurs des transitions L et M nous avons obtenu un système surdéterminé de 29 équations à 13 inconnues, les 13 largeurs des niveaux atomiques L_1 à N_5. Pour l'uranium, une méthode identique a été appliquée, complétant une série de mesures antérieures de transitions L par la mesure complémentaire de 12 transitions M. Les résultats obtenus pour les largeurs naturelles des états L_1 à N_5 de ces deux éléments lourds ont fait l'objet d'une publication [Phys. Rev. A 61 (2000) 012507].

De l'étude faite pour le thorium et l'uranium, il ressortit qu'un des plus grands écarts entre les prévisions théoriques et nos valeurs expérimentales était observé pour le niveau atomique $2s_{1/2}$. D'autre part, une publication récente faisant la synthèse des résultats expérimentaux concernant les largeurs naturelles des états atomiques $1s_{1/2}$ à $4f_{7/2}$ montrait que très peu de données autres que celles déduites de mesures de transitions Coster-Kronig existaient pour la sous-couche L_1 dans le domaine du Tableau périodique compris entre le baryum (Z=56) et le thorium (Z=90). Une seconde étude visant à combler le manque de données précité a donc été entreprise. Principalement parce que la largeur des sous-couches M_4 et M_5 était connue avec une bonne précision, la largeur naturelle de la sous-couche L_1 a été déterminée à partir des transitions quadrupolaires L_1-M_4 et L_1-M_5, ceci pour les éléments $_{62}$Sm, $_{67}$Ho, $_{70}$Yb, $_{74}$W, $_{78}$Pt, $_{80}$Hg et $_{83}$Bi. Les mesures des trois éléments les plus lourds ont été réalisées avec le spectromètre DuMond, celles des autres éléments avec le spectromètre von Hamos. Malgré la difficulté du projet due essentiellement à la faible intensité des transitions L_1-$M_{4,5}$ et la proximité de plusieurs transitions dipolaires plus intenses, celui-ci a pu être mené à bon port. De cette étude ressortit en particulier que pour deux des trois éléments appartenant aux Terres rares, le niveau $2s_{1/2}$ était élargi

par un effet de « splitting » dû au couplage du spin intrinsèque de la lacune 2*s* avec celui du niveau 4*f*. Cette seconde étude a été acceptée pour publication dans Physical Review A.

Variation de l'effet de « shake » dans la couche *L* de l'argon en fonction de l'énergie d'excitation

Lors de la création d'une lacune profonde par effet photo-électrique, le potentiel atomique varie brusquement à cause du rapide changement de l'effet d'écran électronique. Si le changement est plus rapide que le temps de relaxation atomique, un second électron lié peut être soit éjecté dans le continu, soit transféré dans une sous-couche plus extérieure incomplète. Dans le premier cas on parle de processus de « shakeoff », dans le second de « shakeup ». Dans les deux cas, bien que l'effet photo-électrique ne traduise l'interaction d'un photon qu'avec un seul électron, on assiste par l'intermédiaire de l'effet de « shake » à la création d'une deuxième lacune profonde. La probabilité pour qu'un effet de « shake » se produise dépend de l'énergie du photon incident. Cette probabilité augmente à partir de l'énergie de seuil pour atteindre une valeur de saturation lorsque l'énergie du photo-électron *K* est environ 10 fois plus grande que l'énergie de liaison de l'électron subissant l'effet de « shake ». Une meilleure compréhension des mécanismes intervenant dans un effet de « shake » peut donc être obtenue en mesurant la variation du nombre de doubles lacunes profondes créées en fonction de l'énergie des photons incidents. Comme indiqué précédemment, le nombre relatif d'atomes doublement excités par rapport au nombre d'atomes une fois ionisés peut être mesuré à partir de l'intensité relative des rayons X satellites. L'effet de « shake » diminuant avec *Z*, un élément léger, l'argon, a été choisi. Le choix d'un gaz permettait en outre d'éliminer les effets chimiques qui, dans les éléments métalliques légers, peuvent influencer la position et la forme spectrale des raies. L'étude a donc porté sur l'effet de « shake » dans la couche *L* de l'argon résultant de la photoionisation *K* et sur la variation de cet effet en fonction de l'énergie d'excitation.

Le spectre d'émission $K\alpha$ de l'argon excité au moyen de photons monoénergétiques dont l'énergie était comprise entre 3455 et 6540 eV a été mesuré avec le spectromètre von Hamos. Les mesures ont été réalisées auprès de la source de lumière synchrotronique européenne (ESRF), à Grenoble. Les probabilités de « shake » ont été déduites à partir de l'intensité relative des satellites $K\alpha_{1,2}L^{(1)}$ par rapport à la ligne diagramme $K\alpha_{1,2}L^{(0)}$. Les probabilités expérimentales obtenues ont été comparées aux valeurs théoriques prédites par le modèle de Thomas et celui de Roy. Un bon accord a été observé avec les deux modèles. D'autre part, les énergies de seuil pour l'excitation double 1*s*2*p* et 1*s*2*s* ont pu être extraites des mesures ainsi que le rayon r_{max} correspondant à la densité radiale maximale de l'orbitale 2*p* de l'ion Ar^{1+}. Dans les deux cas, les valeurs obtenues sont assez bien reproduites par des calculs MCDF (Multi-Configuration Hartree-Fock). Les résultats de cette troisième partie de la thèse ont été soumis récemment pour publication dans Physical Review A.

Abstract

Two different projects related to Atomic Physics are contained in the present Ph.D. thesis. The first project concerns the natural widths of atomic core levels whereas the second one deals with the double *KL* excitation of gaseous argon resulting from impact with monoenergetic photons.

The first project itself is divided in two parts : the first one is an experimental study of the L_1 to N_5 atomic level widths of two heavy elements, namely thorium and uranium. The second one deals with the natural width of the $2s_{1/2}$ level in several elements ranging between samarium ($Z = 62$) and bismuth ($Z = 83$). In both parts the condition to get reliable results was to use a detecting device whose instrumental broadening was comparable to the investigated widths i.e. in the order of a few eV over the energy domain comprised between 2 keV and 20 keV. This condition could only be satisfied by using crystal spectrometers.

In the second project, the experimental method consisted in comparing the energies and intensities of the transitions $1s^1 2s^2 2p^5 \rightarrow 1s^2 2s^2 2p^4$ and $1s^1 2s^1 2p^6 \rightarrow 1s^2 2s^1 2p^5$ to those of the transition $1s^1 2s^2 2p^6 \rightarrow 1s^2 2s^2 2p^5$. Due to the spectator vacancy $2s$ or $2p$, the $K\alpha_{1,2}L^{(1)}$ satellite x-ray lines corresponding to the two first transitions are shifted to higher energies relative to the $K\alpha_{1,2}L^{(0)}$ diagram lines corresponding to the third transition. From the satellite-to-diagram line yield ratio the double excitation probability can be deduced, provided that the satellites can be resolved from the parent diagram line. Since in argon this energy difference is only about 20 eV, again the feasibility of this project required the use of a crystal spectrometer.

High-resolution x-ray spectroscopy represents thus the common denominator of the two projects. More details about the latter are given below.

Atomic level widths

Precise and reliable data concerning atomic level widths are of interest in both theoretical and experimental physics. For theory such data are important to probe the goodness of theoretical predictions concerning total vacancy lifetimes, radiative and radiationless transition probabilities, or fluorescence yields. Atomic level widths and related x-ray linewidths are also of value in experimental physics. Here a precise knowledge of x-ray linewidths leads to a better accuracy in x-ray emission techniques such as x-ray fluorescence (XRF) and particle-induced x-ray emission (PIXE). Furthermore, in a variety of experiments in which weak structures like Radiative Auger Emission (RAE) lines or satellite x-rays have to be extracted from the tails of close-lying and much more intense diagram transitions, the line shapes of the latter must be known accurately to obtain reliable results. In this case, precise linewidths permit one to improve data analysis by diminishing the number of free fitting parameters and anchoring the natural linewidths of the observed transitions to known values.

Experimental information concerning the widths of L transitions in heavy elements is scarce because the energies of these transitions are rather unfavorable for crystal diffractometry measurements. Transmission-type crystal spectrometers are indeed operated mostly above 20 keV, while reflection-type ones are generally used below 8-10 keV. However, the DuMond transmission-type bent crystal spectrometer of Fribourg permits to measure x-rays with energies down to about 11 keV. This has been made possible thanks to the successful bending of crystal plates only 0.5 mm thick and the wide angular domain (± 20 degrees) that can be scanned by this instrument. Taking advantage of these properties, more than 30 photoinduced L-transitions of solid thorium could be measured. The energies and linewidths of these transitions were determined with high accuracy. As the natural width of an x-ray line represents the sum of the widths of the initial and final atomic states of the transition, it is possible in principle to determine the widths of atomic levels from the observed linewidths of a series of transitions. To apply successfully this method to thorium, additional measurements of 10 M x-ray lines were necessary. The latter were performed with a von Hamos reflecting-type curved crystal spectrometer. From the linewidths of the measured L and M x-ray lines a set of 29 simultaneous equations with the level widths L_1 to N_5 as unknowns was built and resolved by means of a least-squares method. The same method was applied to uranium, adding the linewidths of 12 M x-ray lines to the set of L x-ray linewidths determined in a former study. The results of this project have been published [Phys. Rev. A 61 (2000) 012507].

In the thorium-uranium study the biggest deviation between theory and experiment was observed for the subshell L_1. In addition, a recent comprehensive paper concerning L_1 to N_7 atomic level widths for elements across the Periodic Table revealed a serious lack of modern experimental information for the same level in the region $56 \leq Z \leq 90$. A new project was thus undertaken with the aim to get reliable $2s_{1/2}$ level widths in this region. As the widths of the levels M_4 and M_5 are known with a good precision, the L_1 widths were determined from the quadrupole-allowed L_1-M_4 and L_1-M_5 transitions. Metallic $_{62}$Sm, $_{67}$Ho, $_{70}$Yb, and $_{74}$W were measured with the von Hamos spectrometer whereas $_{78}$Pt, $_{80}$Hg and $_{83}$Bi were measured with the DuMond spectrometer. The project could be completed successfully despite several difficulties arising principally from the extremely weak intensity of the L_1-$M_{4,5}$ transitions and the presence in the observed spectra of close-lying strong dipole transitions. Whereas an excellent agreement with results from Coster-Kronig measurements was observed for the five heaviest elements, an intriguing discrepancy was found for holmium and samarium. The deviations were explained by a splitting effect of the L_1 subshell resulting from the coupling of the $2s$ electron spin in the initial excited state with the total spin of the open $4f$ level. The paper related to this study has been accepted for publication in Physical Review A.

Energy dependent *L*-shell-electron shake in argon following 1*s* photoionization

Atomic inner-shell photoionization is a rather weak process, in a perturbation sense, in which a single photon can be assumed to interact with a single bound electron. One would thus expect that multi-electron excitation caused by photoionization is negligibly small. However, due to the sudden change of the atomic potential following the removal of a core electron by the photon impact, other electrons can be ejected into the continuum (shakeoff) or promoted to higher unfilled bound states (shakeup). The shake probability increases with the energy of the incident photon, varying from zero at the threshold energy up to a saturation value. The latter is attained when the energy of the photoelectron is about ten times bigger than the binding energy of the shaken electron. The result of a shake effect is the creation of a second core-vacancy in the singly-ionized atom (shakeup) or doubly-ionized atom (shakeoff). A better understanding of the mechanisms involved in the shake process can thus be gained by measuring the number of double core-vacancy states produced as a function of the energy of the incident photon beam. As mentioned before, the relative number of doubly-excited states relative to the number of singly-ionized states can be determined from the relative intensity of x-ray satellites. As the shake effect diminishes with *Z*, a light element, argon, was chosen. The choice of argon was further motivated by the fact that the x-ray emission from gases is not affected by chemical and solid state effects. The objective of our study was thus to investigate the variation of the Ar *L*-shell shake probability as a function of the excitation energy from threshold to saturation.

The $K\alpha$ x-ray emission of argon irradiated by monoenergetic photons with energies 3455 eV ≤ E ≤ 6540 eV was measured with the von Hamos spectrometer. The measurements were performed at the European Synchrotron Radiation Facility (ESRF) in Grenoble, France. The shake probabilities were determined from the satellite-to-diagram line yield ratios $I(K\alpha_{1,2}L^{(1)})$: $I(K\alpha_{1,2}L^{(0)})$. The so-obtained experimental probabilities were compared to theoretical predictions based on the model of Thomas and the one of Roy. A good agreement was observed for the two models. From the fit of the model of Thomas to our data, the threshold energies for double 1*s*2*p* and 1*s*2*s* excitation could be determined. The same holds for the radius r_{max} (radius for which the squared radial wave function peaks) of the orbital 2*p* in ionic Ar^{1+}. The values found for the threshold energies and the radius r_{max} were found to be reasonably well reproduced by multi-configuration Hartree-Fock calculations. Results of this shake study were submitted recently for publication in Physical Review A.

L_1 to N_5 atomic level widths of thorium and uranium as inferred from measurements of L and M x-ray spectra

P.-A. Raboud, J.-Cl. Dousse, J. Hoszowska,* and I. Savoy

Departement of Physics, University of Fribourg, Ch. du Musée 3, CH-1700 Fribourg, Switzerland

High-resolution measurements of the photoinduced L and M x-ray spectra of metallic thorium and M x-ray spectrum of metallic uranium were performed with transmission-type and reflection-type bent-crystal spectrometers. Linewidths of 31 L and 10 M x-ray emission lines of thorium and of 12 M x-ray emission lines of uranium were extracted. Using these results and those of Hoszowska *et al.* [Phys. Rev. A **50**, 123 (1994)] for the L x rays of uranium, by means of a least-squares method we have determined the level widths of the subshells L_1 to N_5 of thorium and uranium.

PACS number(s) : 32.30 Rj, 32.70 Jz, 32.80 Fb

I. INTRODUCTION

Atomic level widths and related x-ray linewidths are of interest and value in several respects. For high-resolution x-ray spectroscopy, a precise knowledge of x-ray linewidths is very helpful because it permits one to improve data analysis by diminishing the number of free-fitting parameters and anchoring the natural linewidths of the observed transitions to known values. This results in improved accuracy in x-ray emission techniques such as high-resolution x-ray fluorescence and particle-induced x-ray emission [1-3]. Furthermore, in a variety of experiments in which weak structures have to be extracted from the tails of close-lying and much stronger diagram transitions, the line shapes of the latter must be known accurately to obtain reliable results. Radiative Auger transitions [4-8] are examples of such weak structures sitting on the low-energy tails of intense diagram lines. Satellite x rays that originate from the radiative decay of multiple-vacancy states are often poorly separated from their parent diagram line. In this case, also, the energy and yield of the satellite line can be fitted in a reliable way only if the width of the Lorentzian representing the natural line shape of the neighboring main line is known precisely [9]. As shown in Ref. [10], even in low-resolution Si(Li) spectra, the lifetime broadening inherent to atomic transitions make a significant contribution to the low- and high-energy tails of the peaks. A high-precision fit of such spectra again needs a good knowledge of the natural broadening. Accurate and reliable experimental data concerning atomic

* Present address: European Synchrotron Radiation Facillty (ESRF), 156 rue des Martyrs, F-38043 Grenoble, France.

level widths are also important because they provide a sensitive test of theoretical models. In particular, they are of interest to probe the goodness of theoretical predictions concerning total vacancy lifetimes, radiative and radiationless transition probabilities, or fluorescence yields. In some calculations they are also used to adjust the parameters of the theoretical model. Precise results for the linewidths of L and M x rays are scarce and discrepancies exist between the few existing experimental data and the theoretical predictions. Experimentally reliable results can only be obtained with instruments whose resolution is comparable to the natural linewidths of the transitions to be measured. In x-ray spectrometry this restricts the choice of instruments to crystal spectrometers. The lack of accurate experimental data concerning L x rays of heavy elements is probably due to the fact that the photon energy region between 10 and 20 keV is rather unfavorable for crystal diffractometry measurements. Transmission-type crystal spectrometers are operated mostly above 20 keV, while reflection-type ones are generally used below 10 keV. Crystal spectrometers are characterized by high resolution and high precision. Their luminosity, however, remains small as compared to semiconductor detectors. For M x rays high-resolution crystal spectroscopy is therefore handicapped by the poor intensity of the M x-ray emission lines. Even for heavy elements, the fluorescence yields for the M shell is indeed about 100 times smaller than for the K shell.

In this paper we report on the natural widths of the L_1 to N_5 atomic levels in metallic thorium and metallic uranium. The level widths were obtained from the natural linewidths of a number of L and M x-ray lines measured by means of high-resolution crystal spectroscopy. From the transition widths determined in the present experiment and the L x-ray linewidths obtained for uranium in a similar previous work [11] two self-consistent sets of simultaneous equations with the level widths as unknowns could be built for thorium and uranium. Assuming that core level are only weakly influenced by nonlifetime broadening effects, the natural widths of the levels L_1 to N_5 were then determined by solving the sets of linear equations by means of a least-squares method. Results given in the present paper are not, however, solely limited to the widths of atomic levels. Linewidths and energies of numerous L x-ray lines of thorium and M x-ray lines of thorium and uranium are also presented. To our knowledge, the natural linewidths of most transitions were determined experimentally for the first time. The results obtained in the present work are compared to other experimental data, where available, and theoretical predictions based principally on the independent-particle model.

II. EXPERIMENT

The measurements of the x-ray spectra were performed at the University of Fribourg by means of high-resolution x-ray spectroscopy. The L x-ray emission spectrum of thorium was observed with a Dumond transmission-type crystal spectrometer. As this instrument cannot be used for photon energies below about 10 keV, the M x-ray emission lines of thorium and uranium were measured with a von Hamos

reflection-type crystal spectrometer. For both elements, the fluorescence x-ray spectra were produced by irradiating the targets with the bremsstrahlung of an x-ray tube.

A. *L* x-ray emission spectrum of thorium

The main characteristics of the DuMond curved crystal spectrometer of Fribourg were already presented in several previous papers (see e.g. [6,7,11,12]). Thus, in the following, only the features specific to the experimental setup used for the measurement of the *L* x-ray emission spectrum of thorium will be discussed.

The spectrometer was operated in a so-called modified DuMond slit geometry. In this geometry the target is viewed by the bent crystal through a narrow slit located on the focal circle. The 0.1-mm-wide vertical rectangular slit was made of two 5-mm-thick juxtaposed Pb plates. A 25-mm-high by 4-mm-wide by 0.5-mm-thick self-supported metallic target of thorium was used. The target *L* x-ray emission was induced by means of a Au x-ray tube operated at 80 kV and 35 mA. The distance between the tube anode and the target center was 4.5 cm, and the axis of the conical beam emitted by the x-ray tube was perpendicular to the target-crystal direction. In order to avoid a contamination of the thorium spectrum due to a coherent scattering by the target of a number of characteristic Au *L* x-ray lines from the tube anode, a 250 mg/cm^2-thick aluminium absorber was placed between the tube and the target for the measurements of the L_3-M_1, L_3-M_4 and L_3-M_5 transitions of thorium.

For the diffraction of the x rays the (110) reflecting plane of a 10 × 10-cm^2 quartz-crystal plate, 0.5 mm thick, were used. The quartz lamina was bent to a radius R = 311.1 cm by means of a bending device similar to the one described in Ref. [13]. The effective reflecting area of the crystal was 12 cm^2. The Bragg angles, i.e., the angles between the incident x-ray radiation and the reflecting planes of the crystal, were measured by means of an optical laser interferometer with a precision of 3-5 marsec [14].

The instrumental response of the spectrometer which depends mainly on the slit width and precision of the crystal curvature was determined by measuring the $K\alpha_1$ transition of Au whose energy and natural linewidth were taken from Ref. [15]. From this calibration measurement the instrumental angular broadening was found to be well reproduced by a Gaussian profile of 15.2 arcsec full width at half maximum (FWHM). Over the energy range covered by the *L* x-ray lines of thorium the corresponding energy resolution of the spectrometer varied thus between 3.5 eV for the L_3-M_1 transition (11.118 keV) and 12.1 eV for the L_1-$P_{2,3}$ transition (20.450 keV).

In the DuMond slit geometry, the best angular resolution is obtained when the slit-to-crystal distance is adjusted for each x-ray line. However, when the x-ray spectrum extends over a large angular range and comprises many weak lines, this optimization is not so convenient. It is more practical to measure a selected group of lines with an average value of focusing distance. As a consequence, only a slightly worse instrumental resolution results. In fact the smooth variation of the instrumental broadening as a function of the focusing distance was determined with the Au $K\alpha_1$

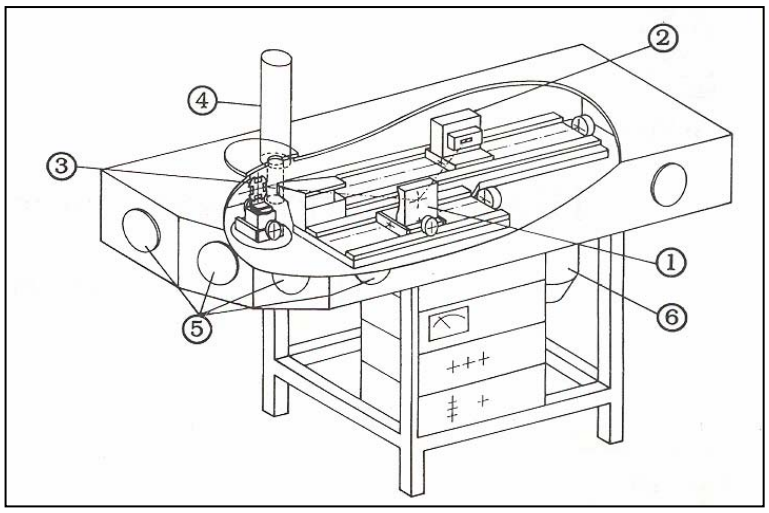

FIG 1. Schematic view of the von Hamos spectrometer : (1) crystal, (2) CCD detector, (3) target barrel, (4) x-ray tube, (5) beam ports and (6) vaccum pump

transition, and then used to compute the actual instrumental width corresponding to each particular thorium *L* x-ray line.

For the energy calibration of the spectrum, the lattice spacing constant of the (110) reflecting planes and the angular position of the zero Bragg angle are needed. The lattice spacing constant was deduced from the above-mentioned $K\alpha_1$ line of Au measurement, giving a value of 2.456624(7) Å. The zero Bragg angle may change when varying the focusing distance. For that reason, it was determined for each group of lines observed at the same focusing , by measuring the most intense line of the group at positive and negative Bragg angles.

For the detection of the x rays a 5-in.-diam. by 0.25-in. NaI(Tl) by 2-in. CsI(Tl) Phoswich (The Harshaw Chemical Co., Crystal and Electronic Products Dept., OH 94139) scintillation detector was employed. This type of detector strongly reduces the Compton noise arising from high-energy photons [11]. A further reduction of the background was achieved by enclosing the Phoswich detector in heavy Pb-Cu-Al shielding, and by sorting on line the events of interest as a function of their energy. In order to reduce the absorption of the x rays in air, evacuated tubes were mounted between the target and the crystal and between the crystal and the 66-cm-long Soller-slit collimator. The latter and the target chamber were also pumped down to about 1 mbar.

B. *M* x-ray emission spectra of thorium and uranium

As the observation of photons below 10 keV requires a reflecting-type x-ray spectrometer, the measurements of the *M* x-ray emission spectra of thorium and uranium were performed with a von Hamos curved crystal facility [16]. The principal elements of this instrument are an x-ray source defined by a rectangular slit, cylindrically bent crystal, and a position-sensitive detector (see Fig. 1). In the von Hamos geometry the crystal is bent around an axis which is parallel to the direction of dispersion, and provides focusing in the nondispersive direction. For a fixed position of

the components, the impact coordinate on the detector of a reflected x-ray corresponds geometrically to a particular Bragg angle, and hence to a particular photon energy. Such a geometry, at one position of the spectrometer components, permits data collection over an energy bandwidth which is limited by the detector length. In order to study a greater energy interval, the central Bragg angle is adjusted by translation of the crystal and correspondingly of the detector along their axes. The slit-to-crystal and crystal-to-detector distances are varied but kept equal. The target, crystal, and detector are all contained in a 180 × 62 × 24.5-cm^3 stainless steel vacuum chamber, which can be pumped down to about 10^{-7} mbar by a turbomolecular pump.

The Bragg angle domain covered by the von Hamos spectrometer extends from 24.4° to 61.1°, so that two different crystals were needed for the coverage of the ~ 6-keV-wide energy domain corresponding to the *M* x rays of thorium and uranium. A $(1\bar{1}0)$ quartz crystal ($2d$ = 8.5096 Å) was employed for the observation of the transitions below 3.5 keV, and a (200) LiF crystal ($2d$ = 4.0280 Å) for transitions at higher energies. Both crystals, 10 cm high by 5 cm wide by 0.5-mm-thick, were glued to Al blocks machined to a precise concave cylindrical surface with a nominal bending radius of 25.4 cm.

The vertical rectangular slit consisted of two juxtaposed Ta pieces 0.3 mm thick and 10 mm high. The slit width was 50 μm for all measurements. A 25-mm-high by 4-mm-wide metallic target of natural uranium, 48 mg/cm^2 thick, and a 24-mm-high by 10-mm-wide metallic target of thorium, 575 mg/cm^2 thick, were used. The target *M* x-ray emission was induced by means of a Cr anode x-ray tube operated at 60 kV and 40 mA.

The x rays were recorded with a CCD (charged-couples device) position-sensitive detector 27.65 mm long and 6.9 mm high, having a depletion depth of 50 μm and consisting of 1024 columns and 256 rows with a pixel size of 27 × 27 μm^2. The diffracted x rays hitting the CCD build a two-dimensional pattern on the detector plane. The horizontal axis of the detector corresponds to the energy axis of the x-ray spectrum, while the vertical extension of the detector serves mainly to collect more intensity. The CCD detector was thermoelectrically cooled down to -60° C. It was operated by a ST-138 controller (Princeton Instrument, Inc.) equipped with a DMA/TAXI high-speed serial interface which can sustain data transfer to a personal computer at 1 Mbyte/sec.

For data acquisition and analysis of images, a dedicated software package written specifically to operate the ST-138 controller was used. The time of a single acquisition was chosen depending on the count rate, so that multiple hits on one pixel were minimized. Thanks to the good energy resolution of the CCD detector, higher-order reflections and background events could be rejected by setting appropriate energy windows. The data were taken in a repetitive accumulation mode. Each image corresponding to a separate acquisition was filtered. Then the different images were summed and the resulting two-dimensional spectrum was projected on the axis of dispersion to give the one-dimensional position spectrum.

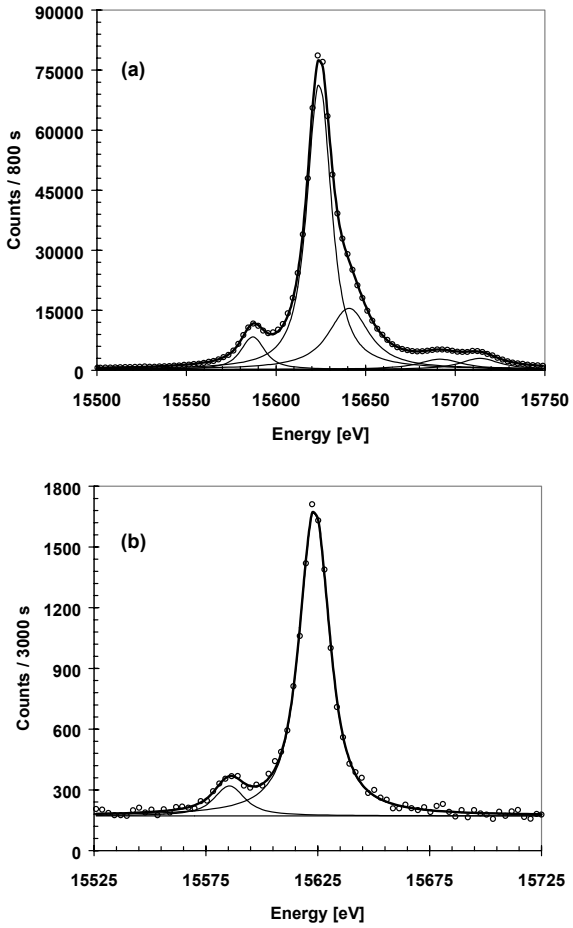

FIG. 2. The L_3-N_4 (15587 eV), L_3-N_5 (15624 eV) and L_1-M_2 (15640 eV) transitions of thorium with the accompanying M satellite structure components shifted by 68 and 90 eV with respect to the L_3-N_5 line. The L emission was induced with the x-ray tube operated at (a) 80 and (b) 20.4 kV

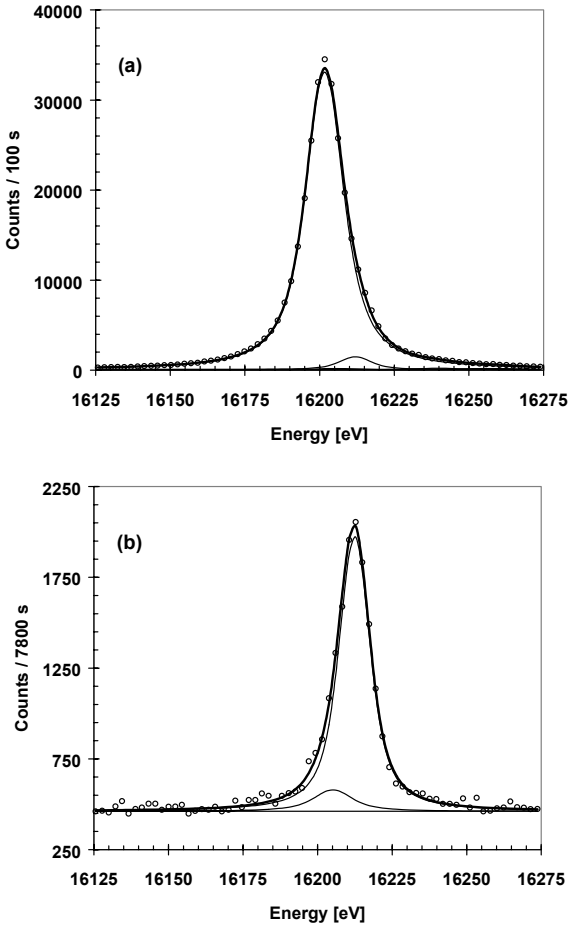

FIG. 3. The L_2-M_4 (16202 eV) and L_3-$O_{4,5}$ (16205 eV and 16212 eV) transitions of thorium. The L emission was induced with the x-ray tube operated at (a) 80 and (b) 19.6 kV

III. DATA ANALYSIS

The energy calibration of the spectrometer and the determination of the instrumental response were performed by measuring the $K\alpha_1$ x-ray lines of Ar, Ca, Sc, Ti and V. The natural linewidth and energies of the K transitions were taken from Refs. [17,18], respectively. It was found that for both crystals the instrumental response could be well reproduced by a Gaussian profile whose width (FWHM) varied as a function of the x-ray energy between 1.0 and 1.3 eV.

The L and M x-ray spectra were analysed by means of the least-squares-fitting computer code MINUIT [19]. As the convolution of the Gaussian instrumental broadening with the Lorentzian representing the natural line shape of an x-ray transition results in a so-called Voigt function, such Voigt profiles were employed to fit the observed spectral lines. The natural widths of the x-ray lines of interest were extracted by keeping fixed in the fit the known Gaussian experimental broadening. The energies and intensities of the transitions as

well as the linear background were used as additional free fitting parameters.

The M and N satellite structures observed on the high-energy tails of the L_3, respectively M_3 to M_5 diagram transitions could also be fitted satisfactorily with Voigt functions. However, because these satellite structures consist in general of numerous overlapping components many of them had to be fitted with several Voigt profiles. Average energy shifts of L x rays due to M spectator vacancies are reported in Ref. [20]. We have used these theoretical predictions in the analysis to identify the satellites accompanying the observed L_3 x rays lines. A clear example of M satellite structure can be seen on the high-energy side of the L_3-N_5 transition represented in Fig. 2(a).

In certain spectra a strong overlap of distinct diagram lines made the analysis more difficult and the results of the latter less reliable. Such problems were encountered, for instance, in the fit of the L x-ray spectrum of thorium with the close-lying L_3-$N_{4,5}$ and L_1-M_2 transitions [see Fig. 2(a)] and L_2-M_4 and L_3-$O_{4,5}$ transitions [see Fig. 3(a)]. The energy differences between the two lines are both cases smaller than the natural widths of the overlapping transitions. The difficulty was solved in the following way. First, the problematic energy regions were remeasured by operating, the x-ray tube at 20.4 [see Fig. 2(b)] and 19.6 [see Fig. 3(b)] kV, respectively, i.e. at voltage values just below the L_1 and L_2 edges of thorium. These spectra could then analyzed properly since they were no longer affected by the overlap problem. Finally, the 80-kV spectra could also be fitted successfully by keeping the energies and linewidths of the L_3 transitions at the values obtained from the analysis of the 20.4- and 19.6-kV spectra fixed in the fitting procedure.

IV. RESULTS AND DISCUSSION

A. *L* x-ray lines of thorium

The values of the natural linewidths and energies of the 31 L x-ray transitions of thorium observed in the present study are listed in Tables I and II, respectively. Our results are compared to other available experimental data and theoretical predictions. The theoretical x-ray linewidths were determined from the sum of the widths of the two levels involved in the transitions, using results of McGuire's calculations [21-23] for L, M and N atomic level widths. It has to be noted that the errors quoted in Tables I and II are only statistical errors obtained from the error matrix of the least-squares-fit program, and that they do not include the smaller but not vanishing systematic errors inherent to the experimental method and instruments employed in our investigations.

From Table I one can notice first that existing experimental information about the natural linewidths of L x-ray transitions in thorium is rare and concerns only the most intense lines. The values quoted in the third column were taken from the tabulation of Salem and Lee [17]. They are based on relatively old measurements performed in 1961 by Merill and DuMond [24] with a double-crystal spectrometer. Errors concerning these measurements were not reported, but they were estimated by Salem and Lee to be 10% or more. The average of the absolute values of the differences between our results and those of

TABLE I. Natural linewiths in (eV) of photoinduced *L* x-ray emission lines of thorium. Our experimental results are compared to existing experimental data (Expt.) and theoretical predictions (Calc.)

Lines	This experiment	Ref. [17] Expt.	Ref. [25] Expt.	Ref. [21-23] Calc.
L_1-M_2	27.6 ± 0.7	26.4		35.9
L_1-M_3	23.6 ± 0.3	22.9	21.5	33.3
L_1-M_4	17.6 ± 0.5			23.6
L_1-M_5	17.0 ± 0.3			23.3
L_1-N_2	22.3 ± 0.1			28.7
L_1-N_3	20.4 ± 0.1			27.9
L_1-N_4	16.1 ± 2.5			25.7
L_1-N_5	16.8 ± 1.6			25.7
L_1-O_2	22.2 ± 1.2			
L_1-O_3^{I}	22.8 ± 1.2			
L_1-O_3^{II}	18.9 ± 0.6			
L_1-$O_{4,5}$	13.8 ± 2.3			
L_1-$P_{2,3}$	19.9 ± 0.6			
L_2-M_1	23.1 ± 0.2			34.0
L_2-M_4	11.6 ± 0.1	12.4	11.2	14.5
L_2-M_5	11.7 ± 2.4			14.2
L_2-N_1	19.2 ± 0.4			22.5
L_2-N_4	13.3 ± 0.1	15.0	14.4	16.6
L_2-N_6	8.6 ± 0.6			11.5
L_2-O_1^{I}	29.9 ± 0.2			
L_2-O_1^{II}	29.4 ± 0.5			
L_2-O_4	8.5 ± 0.1			
L_3-M_1	23.5 ± 0.5		24.3	29.7
L_3-M_4	11.8 ± 0.1	11.9	11.8	10.2
L_3-M_5	12.0 ± 0.1	11.8	11.8	9.9
L_3-N_1	19.3 ± 0.1			18.2
L_3-N_4	12.1 ± 0.2			12.2
L_3-N_5	12.5 ± 0.1	12.8	12.7	12.2
L_3-N_6	7.6 ± 1.2			7.1
L_3-N_7	7.6 ± 0.7			
L_3-O_1^{I}	26.0 ± 2.2			
L_3-O_1^{II}	23.5 ± 2.4			
L_3-O_4	12.3 ± 4.0			
L_3-O_5	8.3 ± 0.3			

Merill and DuMond is only 0.7 eV or 5%, thus indicating that already in these pioneering works of crystal spectroscopy remarkable results were obtained. A similar good agreement is observed between our results and the experimental values published more recently by Amorim *et al.* [25]. In this case the mean value of the relative differences is about 4%. In contrast to that, a comparison with the values listed in the last column on the right seems to indicate that the theory is in disagreement with our results. However, if we

TABLE II Energies in (eV) of photoinduced *L* x-ray emission lines of thorium. Our experimental results are compared to the data from two experiments (Expt.) and one theory (Calc.)

Lines	This experiment	Expt.Ref. [18]	Expt.Ref. [32]	Calc.Ref. [33]
L_1-M_2	15639.64 ± 0.35	15642.9	15639.5	15641.0
L_1-M_3	16423.96 ± 0.07	16425.8	16424.0	16426.0
L_1-M_4	16980.37 ± 0.21	16981.0	16979.4	16981.0
L_1-M_5	17139.00 ± 0.12	17139.0	17138.0	17140.0
L_1-N_2	19303.00 ± 0.04	19305.0	19301.8	19304.0
L_1-N_3	19503.57 ± 0.06	19507.0	19502.5	19504.0
L_1-N_4	19756.88 ± 0.83	19755.0	19755.7	19758.0
L_1-N_5	19794.04 ± 0.50	19794.0	19793.7	19795.0
L_1-O_2	20236.52 ± 0.18	20242.0	20245.0	20243.0
L_1-O_3^{I}	20272.10 ± 0.66			
L_1-O_3^{II}	20290.66 ± 0.27	20292.0	20288.2	20288.2
L_1-$O_{4,5}$	20381.03 ± 0.97	20383.0		
L_1-$P_{2,3}$	20450.39 ± 0.28	20424.0	20426.0	
L_2-M_1	14510.42 ± 0.08	14509.0	14509.8	14511.0
L_2-M_4	16201.99 ± 0.02	16202.2	16201.4	16202.0
L_2-M_5	16358.20 ± 1.00	16359.0	16360.0	16361.0
L_2-N_1	18364.47 ± 0.11	18370.0	18362.3	18363.0
L_2-N_4	18978.38 ± 0.02	18982.5	18977.7	18979.0
L_2-N_6	19348.12 ± 0.15	19353.0	19347.9	19349.0
L_2-O_1^{I}	19395.21 ± 0.32			
L_2-O_1^{II}	19408.89 ± 0.51	19403.0	19402.0	19403.0
L_2-O_4	19597.16 ± 0.02			
L_3-M_1	11118.13 ± 0.18	11118.6	11117.6	11118.0
L_3-M_4	12809.58 ± 0.03	12809.6	12809.2	12810.0
L_3-M_5	12968.02 ± 0.02	12968.7	12967.8	12968.0
L_3-N_1	14973.52 ± 0.05	14975.0	14970.1	14970.0
L_3-N_4	15587.01 ± 0.07	15587.5	15585.5	15586.0
L_3-N_5	15624.06 ± 0.03	15623.7	15623.5	15623.0
L_3-N_6	15955.95 ± 0.55	15964.0	15955.7	15956.0
L_3-N_7	15965.98 ± 0.58	15964.0	15964.9	15965.0
L_3-O_1^{I}	16006.52 ± 0.63	16010.5	16009.8	16010.0
L_3-O_1^{II}	16024.27 ± 0.63			
L_3-O_4	[a]16205.12		16205.4	16205.0
L_3-O_5	16212.40 ± 0.14		16211.7	16213.0

[a] value kept fixed in the fit according to the energy difference determined from the M_3-$O_{4,5}$ transition

consider that the theoretical x-ray linewidths were determined by adding the natural widths of the two levels participating in the transition and that the width of each of these two levels was computed from the sum of the calculated radiative, Auger and Coster-Kronig widths, the observed differences are more understandable. In fact, theory overestimates significantly only

the widths of those transitions in which an *s* level (i.e., an X_1-subshell) is involved. This observation indicates that the Coster-Kronig yields calculated by McGuire are probably too large.

Examining now the values of the experimental linewidths obtained in the present study, one can see that the expected general trend $\Gamma_{L_1Y_k} > \Gamma_{L_2Y_k} \geq \Gamma_{L_3Y_k}$ attributed to the decrease in the Coster-Kronig-Auger decay rates with increasing angular momentum is in general well verified. An important question on which we will focus in the following is to know whether nonlifetime broadening effects influence the natural linewidths of the presently investigated thorium lines and, if yes, to what extent our results are affected by such effects. A review of the possible broadening contributions can be found in Ref. [26]. In our experiment the main contributions are associated with the occurrence of multiple-vacancy states in the decaying atoms, and with exchange interactions between core holes and unpaired valence electrons.

The energy of so-called x-ray satellite lines emitted by atoms which have more than one inner-shell vacancy in their initial and final states is in generally slightly higher than that of the parent diagram x rays which are associated with initial and final states of single-hole configurations. The energy difference between a satellite and its parent diagram line is found to decrease with the principal quantum number of the spectator vacancy, i.e. the vacancy not involved in the transition. As consequence, the radiative decay of *LM* states gives rise to resolved satellites, whereas that of *LN* states results only in a broadening of the parent diagram line. Extensive calculations concerning the energies of *L* x-ray satellites of thorium with one spectator vacancy in the *M* or *N* shell (hereafter called *M* or *N* satellites) can be found in Ref. [27]. The energy shifts of *O* and *P* satellites are much smaller and their influence on the *L* x-ray linewidths can thus be neglected. In other words, our experimental linewidths of *L* transitions may be affected in a sizeable way only by satellites related to spectator vacancies located in the *N* shell.

In photoinduced *L* x-ray spectra, satellite lines may be induced by *LLX* Coster-Kronig transitions and shakeoff processes, while direct multiple ionization can be considered as negligibly small. For thorium, $L_1L_2N_{4\text{-}7}$, $L_1L_3N_{1\text{-}7}$ and $L_2L_3N_{1\text{-}7}$ Coster-Kronig transitions are allowed, from which L_2N_k and L_3N_k doubly ionized states result. Taking into account the probabilities for $L_jL_3N_k$ Coster-Kronig transitions quoted in Ref. [28] and the weighted energy shifts of the N_k satellite components from Ref. [27], we found, for instance, that the average energy shift $E(L_3N^0\text{-}M_1N^0) - E(L_3N^1\text{-}M_1N^1)$ of the *N* satellite of the L_l transition is 3.2 eV. Similarly we found for the average energy shift of the L_l *M* satellite produced, via $L_1L_3M_{4,5}$ Coster-Kronig transitions a value of 39.5 eV which is in quite satisfactory agreement with the value of 36.0 ± 2.0 eV extracted from our measurements. From the fitted relative intensity of the *M* satellite (19%) and the ratio $\sum_{j=1}^{2}\sum_{k=1}^{7} P_{CK}(L_jL_3N_k) \div \sum_{l=4}^{5} P_{CK}(L_1L_3M_l)$ of the Coster-Kronig (CK) probabilities P_{CK} taken from [28], a relative intensity of about 7.5% with respect to the diagram line is expected for the *N* satellite. Assuming furthermore that the width of the *N*

satellite is similar to that of the *M* satellite for which a value of 44 ± 5 eV was obtained from the data analysis, the natural linewidth and energy of the pure L_l diagram transition can be determined by subtracting from the profile the *N* satellite line. The new value obtained for the linewidth is 23.2 eV, i.e. only 0.3 eV smaller than the result given in Table I. The change in the energy is –0.04 eV, which is also negligible with respect to quoted uncertainty of 0.18 eV. It can thus be concluded that the experimental linewidths of the L_3 and *a fortiori* those of the L_2 x rays determined in the present study are only weakly increased by the unresolved *N* satellites originating from Coster-Kronig transitions, the L_1 x rays not being influenced at all by this nonlifetime broadening effect.

In photoionization double-vacancy states may also arise from shake processes. As a consequence of the abrupt change of the atomic potential following the removal of a core electron by photon impact, other bound electrons can indeed be ejected into the continuum (shakeoff) or promoted to higher unoccupied bound states (shakeup). The shakeup to shakeoff probability ratio decrease rapidly with increasing atomic number *Z* so that for heavy elements like thorium only the shakeoff process must be considered. Predictions for shakeoff probabilities in different subshells when a single hole is created in the *L* shell were reported for iridium, gold and uranium in Ref. [29]. The calculations were performed within the frame of the sudden approximation method [30,31]. From an interpolation of the results quoted in Ref. [29], probabilities for shakeoff processes in the *M* and *N* shells of thorium were found to

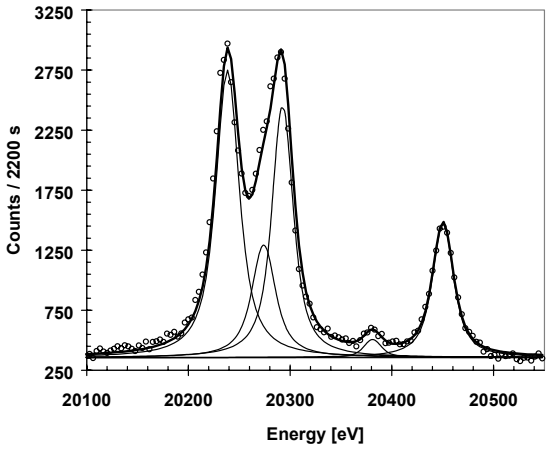

FIG. 4. The L_1-O_2 transition of thorium at 20236 eV, the two splitting components of L_1-O_3 at 20272 and 20291 eV, respectively, and the L_1-$O_{4,5}$ and L_1-$P_{2,3}$ emission lines.

0.13% and 1.84%, respectively. The very small shakeoff probability predicted for the *M* shell is well confirmed by our data which do not reveal any *M* satellite structure for the transitions to the L_1 level nor to the L_2 one [see, e.g., Fig. 3(a)]. The *N* shell shake probability is more than ten times larger but its contribution to the *N* satellite yields can be considered as modest compared to that of *LLN* Coster-Kronig transitions. Broadening and shift of the observed *L* x rays originating from unresolved *N* satellite structures due to shakeoff processes may thus be disregarded.

A further examination of Table I shows that some of the transitions from highest occupied subshells have an unexpectedly large width which cannot be attributed to the effect of multiple vacancy states. Line shape of the *L* transitions from the $5s_{1/2}$ and $5p_{3/2}$ orbitals are particularly influenced by this intriguing effect. As shown in Fig. 4, the L_1-O_3 transition is not only broadened but exhibits also a visible asymmetry on its low energy flank. This asymmetry cannot be associated with *M*

satellite components of the diagram line appearing just below since the latter is the L_1-O_2 transition. The same kind of deformation was observed for the L_3-O_1 line. In both cases, the complex profiles could be well fitted with two Voigtians separated by about 18 eV and labelled *I* and *II* in the Tables. In a previous study concerning the *L* x-ray emission of uranium [11], very similar line shapes were obtained for these two transitions. The observed broadening and splitting of the transitions were interpreted as due to multiplet states formed by the exchange interaction between unpaired valence electrons and the core hole. More detailed information about this effect can be found in the paper by Hoszowska *et al.* [11].

The *L* x-ray energies of thorium determined in our work are listed in Table II. They are all based on the $K\alpha_1$ transition of gold measured in third order of reflection, i.e., at about the same Bragg angle as the transitions of interest. The energy (68804.94 ± 0.18 eV) of this reference line was taken from Ref. [15]. In Table II the quoted uncertainties vary between 0.02 eV (1.2 ppm) for the strongest lines to about 1 eV (60 ppm) for the weakest ones. An additional relative uncertainty of about 3 ppm arising from the crystal lattice constant should be added to these numbers, whereas the errors inherent to the optical laser interferometer can be neglected. For comparison, in Table II we also report experimental values from Bearden [18] and Nordling and Hagström [32], as well as theoretical predictions from Larkins [33]. As Nordling and Hagström data are based on x-ray photoemission (XPS) measurements, the transition energies were computed from the differences of the quoted binding energies. This same holds for the theoretical values from Larkins. In general we see from Table II that for the majority of the lines the three experimental values and theoretical one are consistent within fluctuations of about ± 1 eV. XPS results are, for most transitions, closer to ours than those from Bearden. It is also interesting to note that the calculated energies which reproduce quite well our results are, however, systematically higher by 1 eV or more for the L_1 transitions. This could be an indication that the binding energy of the L_1 level is overestimated by Larkins' calculations. This trend is not observed for the L_2 and L_3 transitions. Furthermore, we can see that out energy of the L_1-O_2 x-ray line is markedly smaller than the two other experimental values, the latter being both more or less consistent with the theoretical energy. Although no asymmetry such as the one observed in the L_1-O_3 and L_3-O_1 transitions could be detected in this line, we are inclined to explain the difference between our result and the three others by the exchange interaction effect mentioned above. The opposite is observed for the energy of the L_1-$P_{2,3}$ transition (Fig. 4), for which we have found a value higher by about 25 eV than the results of Bearden and Nordling and Hagström, but in satisfactory agreement with the theoretical prediction of Larkins. Using the binding energies quoted by Larkins for the P_2 (25 eV) and P_3 (17 eV) levels, energies of 20477 and 20455 eV are indeed obtained for the L_1-P_2 and L_1-P_3 transitions, values which are consistent with the result of 20450.4 eV found in the present work for the unresolved L_1-$P_{2,3}$ lines. For the $P_{2,3}$ doublet

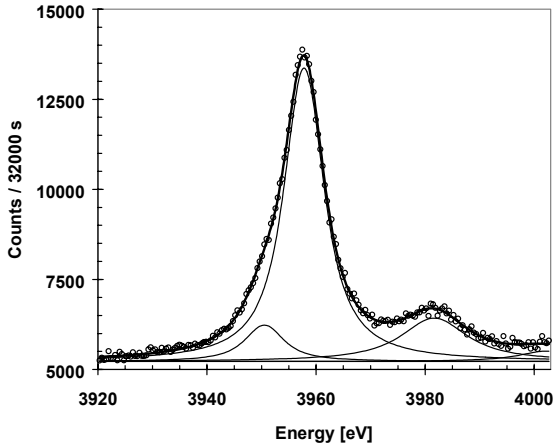

FIG. 5. The M_3-$O_{4,5}$ transitions of thorium at 3951 and 3958 eV, respectively, with the accompanying N satellite structure.

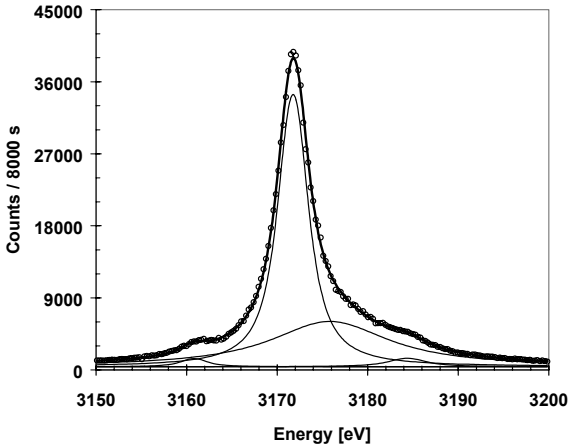

FIG. 6. The M_5-$N_{6,7}$ transitions of uranium at 3161 and 3172 eV, respectively, with the accompanying N satellite structure components shifted by 5 and 13 eV with respect to the M_5-N_7 line.

Nordling and Hagström gave a binding energy of 44 eV which is not confirmed by another more recent XPS measurement [34] from which values of 24.5 and 16.6 eV fully consistent with Larkins' predictions were obtained for the binding energies of the P_2 and P_3 levels. We are thus inclined to believe that the results of Bearden and Nordling and Hagström concerning the energy of the L_1-$P_{2,3}$ transition are erroneous.

B. *M* x-ray lines of thorium and uranium

One of the aims of the present project was the determination of the natural widths of the L_1 to N_5 atomic levels. However, to attain this objective the L x-ray transition widths solely do not suffice. Additional information concerning the widths of the M and N levels is needed. The alternative would be to know the widths of several M x-ray transitions from the N shell. As existing experimental information concerning M and N level widths or M x-ray linewidths is very scarce, our investigations were extended to the high-resolution observation of the M x-ray emission spectra of thorium and uranium. Due to the poor intensity characterising M x rays, we have restricted out measurements to the strongest transitions. M x-ray lines to the M_1 level which are extremely weak (for instance for thorium, the fluorescence yield ω_{M1} is only 4.5×10^{-3} [22]) could unfortunately not be observed for thorium nor for uranium.

For illustration the M_3-$O_{4,5}$ lines of thorium and the M_5-$N_{6,7}$ lines of uranium are depicted in Figs 5 and 6, respectively. It is interesting to note that the M_3-O_4 and M_5-N_6 lines which correspond both to allowed $\Delta j = 0$ $E1$ transitions are much weaker than the parent $\Delta j = 1$ M_3-O_5 and M_5-N_7 transitions. A similar intensity attenuation for $\Delta j = 0$ transitions is observed in L x-ray spectra, as shown, for instance, in Fig. 2 for the L_3-$N_{4,5}$ transitions, but not in K x-ray spectra where $\Delta j = 0$ and 1 transitions have approximately the same transition probabilities. The more or less resolved structures observed on the high-

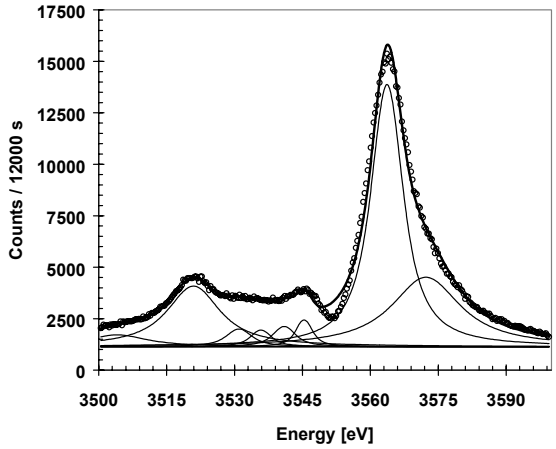

FIG. 7. The M_3-$N_{4,5}$ transitions of uranium at 3521 and 3564 eV, respectively, with the M_3-N_5 N satellite structure at 3572 eV. One can see the influence of the M_5 absorption edge at 3553 eV. The broad structure between the M_3-N_4 line and the absorption edge corresponds to several overlapping transitions (see the text)

energy side of the M_3-O_5 (Fig. 5) and M_5-N_7 (Fig. 6) diagram lines are due to N satellites produced by *MMN* Coster-Kronig transitions and to a smaller extent by shakeoff processes. It was mentioned in Sect. IV A that the energy shifts of the satellites associated with a given diagram line decrease with the principal quantum number of the spectator vacancies. It can also be shown that the satellite energy shifts increase with the principal quantum number of the transition electrons. This explains why the N satellite structure is better separated from the parent diagram line for the $\Delta n = 2$ M_3-O_5 transition than for the $\Delta n = 1$ M_5-N_7 transition.

The complexity of M x-ray spectra and the difficulties encountered in their analysis are well illustrated by Fig. 7, which within a relatively narrow energy domain presents many M x-ray lines of uranium. First one can see, at 3521 and 3563 eV, the M_3-N_4 and M_3-N_5 transitions, respectively. The asymmetry appearing on the high-energy flank of the M_3-N_5 line is due to the N satellite of the latter transition. The small excess of intensity observed on the low-energy side of the M_3-N_4 line was attributed to the M_5-P_1 quadrupole transition, while the flat region between the M_3-N_4 and M_3-N_5 transitions consists of several unresolved lines that were tentatively assigned to the M_3-N_4 N satellite and to the M_4-O_3 and M_5-P_3 transitions. The multiplet splitting found for the L_1-O_3 transition (see Sec. IV A) probably also affects the M_4-O_3 line and thus contributes to the smearing of the spectral lines pertaining to this energy region. Furthermore, the effect of the M_5 edge which results in an enhanced self-absorption of the x rays in the target is clearly visible around 3553 eV, where the experimental data are indeed poorly reproduced by the fit. The line shape of the M_3-N_5 transition is certainly affected by the close-lying M_5 edge. The linewidth obtained from the data analysis for this transition is indeed only 7.5 ± 0.1 eV. This result which is not consistent with the widths of the levels M_3 and N_5 extracted from the other L and M transitions is, in our opinion, not reliable and was therefore not considered in the calculation of the L_1 to N_5 level widths (see Sec. IV C). It can be mentioned that we have not tried to correct the line shape of the M_3-N_5 transition to account for the increased self-absorption because, as observed in Ref. [35], the M_5 edge of U presents a complicated structure due to the resonant excitation of 3*d* electrons into the unfilled 5*f* subshell.

The linewidths and energies of the observed transitions are presented in Tables III and IV

TABLE III. Natural linewidths in (eV) of photoinduced *M* x-ray emission lines of thorium. Our experimental results are compared to theoretical predictions of McGuire

Lines	This experiment	Ref. [22,23] Calc.
M_2-N_4	17.7 ± 0.2	20.8
M_3-N_5	12.1 ± 0.6	18.2
M_3-O_1	40.0 ± 2.1	
M_3-O_4	7.5 ± 0.8	
M_3-O_5	7.7 ± 0.1	
M_4-N_2	16.5 ± 1.4	11.5
M_4-N_6	3.5 ± 0.1	3.4
M_5-N_3	14.3 ± 0.7	10.4
M_5-N_6	3.4 ± 0.2	3.1
M_5-N_7	3.5 ± 0.1	3.1

for thorium and in Tables V and VI for uranium. The instrumental broadening of the von Hamos spectrometer was determined from measurements of several $K\alpha_1$ transitions whose linewidths were taken from Ref. [26]. As this instrumental broadening was small (about 1 eV) as compared to the linewidths of the *M* x rays of interest, the errors (5-10 %) on the widths of the reference $K\alpha_1$ lines were neglected, and are thus not included in Tables III and V. No information concerning the energy shifts of *M* x-ray lines with one spectator vacancy in the *O* and *P* shells could be found in the literature, except for the M_4-N_6 and M_5-N_7 transitions of uranium for which the theoretical energy shifts due to one spectator vacancy in the O_1 and P_1 subshells are reported in Ref. [36]. Values of 0.9 and 0.0 eV and 0.9 and 0.1 eV, are quoted for the two transitions. As these shifts are small as compared to the natural linewidths of the observed *M* transitions, we have assumed that the *O* and *P* satellites do not significantly influence the widths and the energies of *M* x rays. The theoretical linewidths were again obtained from the sum of the widths of the two levels involved in the transition. *M* and *N* levels widths were taken from McGuire's predictions (thorium *M* levels [22], uranium *M* levels [37], and thorium and uranium *N* levels [23]). To

TABLE IV. Energies in (eV) of photoinduced *M* x-ray emission lines of thorium. Our experimental results are compared to the data from two experiments (Expt.) and one theory (Calc.).

Lines	This experiment	Ref. [18] Expt.	Ref. [32] Expt.	Ref. [33] Calc.
M_2-N_4	4116.0 + 0.1 [a]	4117.0	4116.2	4117.0
M_3-N_5	3370.3 ± 0.1 [b]	3370.0	3369.7	3369.0
M_3-O_1	3751.9 ± 0.5 [c]	3780.0	3756.0	3756.0
M_3-O_4	3950.5 ± 0.3 [c]	3959.0	3951.6	3951.0
M_3-O_5	3957.8 ± 0.1 [c]	3959.0	3957.9	3959.0
M_4-N_2	2323.1 ± 0.3 [b]	2322.0	2322.4	2323.0
M_4-N_6	3147.0 ± 0.1 [b]	3145.8	3146.6	3147.0
M_5-N_3	2365.2 ± 0.3 [b]	2364.0	2364.5	2364.0
M_5-N_6	2988.0 ± 0.1 [b]	2987.0	2987.9	2988.0
M_5-N_7	2997.0 + 0.1 [b]	2996.1	2997.1	2997.0

[a] Reference energy : 4090.6 eV (Sc $K\alpha_1$)

[b] Reference energy : 2957.70 eV (Ar $K\alpha_1$)

[c] Reference energy : 3691.68 eV (Ca $K\alpha_1$)

TABLE V. Natural linewidths in (eV) of photoinduced *M* x-ray emission lines of uranium. Our experimental results are compared to existing experimental data (Expt.) and theoretical predictions (Calc.).

Lines	This experiment	Ref. [36] Expt.	Ref. [23,37] Calc.
M_2-N_4	18.1 ± 0.2		24.4
M_2-O_4	18.7 ± 0.3		21.2
M_3-N_1	20.2 ± 0.8		24.4
M_3-N_4	13.4 ± 0.3		16.8
M_3-O_1	38.4 ± 3.2		
M_3-O_4	8.1 ± 1.0		
M_3-O_5	8.2 ± 0.1		
M_4-N_2	15.3 ± 1.0	13 ± 2	11.9
M_4-N_6	3.6 ± 0.1	4.3 ± 0.3	4.7
M_5-N_3	12.8 ± 0.3	15 ± 2	10.8
M_5-N_6	3.6 ± 0.1	4.1 ± 0.6	4.45
M_5-N_7	3.5 ± 0.1	4.1 ± 0.3	4.45

our knowledge experimental information concerning *M* x-ray linewidths does not exist for thorium, whereas for uranium some data were found for the M_4 and M_5 transitions [36].

Regarding the energies, experimental results are available for both thorium and uranium but not for all transitions. As for the *L* x rays the theoretical energies of the *M* x-ray lines were

TABLE VI. Energies in (eV) of photoinduced *M* x-ray emission lines of uranium. Our experimental results are compared to the data from three experiments (Expt.) and one theory (Calc.).

Lines	This experiment	Ref. [18] Expt.	Ref. [36] Expt.	Ref. [38] Expt.	Ref. [33] Calc.
M_2-N_4	4400.8 ± 0.1 [a]	4401.0	4401.0		4401.0
M_2-O_4	5075.9 ± 0.1 [b]	5075.0			5078.0
M_3-N_1	2863.0 ± 0.1 [c]	2863.0	2862.2		2862.0
M_3-N_4	3521.0 ± 0.1 [d]	3521.0	3523.7		3524.0
M_3-O_1	3979.9 ± 0.3 [e]	3980.0			3980.0
M_3-O_4	4195.8 ± 0.4 [e]	4205.0			4201.0
M_3-O_5	4204.2 ± 0.1 [e]	4205.0			4208.0
M_4-N_2	2455.6 ± 0.2 [c]	2454.8	2455.4	2455.7	2455.0
M_4-N_6	3336.7 ± 0.1 [c]	3336.7		3336.7	3336.0
M_5-N_3	2507.0 ± 0.1 [c]	2507.0	2506.6	2506.8	2507.0
M_5-N_6	3160.9 ± 0.1 [c]	3159.5		3160.0	3160.0
M_5-N_7	3171.8 ± 0.1 [c]	3170.8		3171.4	3172.0

[a] Reference energy : 4510.84 eV (Ti $K\alpha_1$)

[b] Reference energy : 4952.20 eV (V $K\alpha_1$)

[c] Reference energy : 2957.70 eV (Ar $K\alpha_1$)

[d] Reference energy : 3691.68 eV (Ca $K\alpha_1$)

[e] Reference energy : 4090.6 eV (Sc $K\alpha_1$)

computed from the binding energies quoted by Larkins [33].

A comparison of the linewidths obtained in our experiment with McGuire's predictions shows that the theoretical values systematically overestimate the widths of the transitions to the M_2 and M_3 levels. This observation may indicate that McGuire's probabilities for M_2M_4X and M_3M_5X Coster-Kronig transitions which are the predominant processes in the decay of M_2 and M_3 vacancies are too large. Thus it seems that the rates of the N_2N_4X and N_3N_5X Coster-Kronig transitions which govern the N_2 and N_3 vacancy lifetimes are underestimated by the calculation of McGuire. This statement is based on the fact that McGuire's predictions for M_4-N_2 and M_5-N_3 transitions are smaller by 3-5 eV than our experimental values, whereas his predictions for the M_4-N_6, M_5-N_6 and M_5-N_7 transitions are in satisfactory agreement with our results. Concerning the experimental linewidths given by Keski-Rahkonen and Krause [36] for two M_4 and three M_5 x-ray lines of uranium, one can see from Table V that relative differences up to 15% are found, but the quoted values are almost consistent with ours within the given experimental uncertainties.

The energies found in the present work for the M x-ray lines of thorium and uranium are based on the energies of different $K\alpha_1$ transitions from several light elements (see Tables IV and VI for details). The errors on the energies taken as references are typically of the order of 10 ppm but they are not included in the uncertainties quoted in Tables IV and VI. Except for the M_3-O_1 transition, our results are remarkably well reproduced by Larkins calculations [33] in the case of thorium. For uranium, the energies of the M_2-O_4, M_3-O_4 and M_3-O_5 transitions are overestimated by the theory by 2-5 eV indicating that the O_4 and O_5 binding energies of Larkins are probably too big. Energies of other transitions, however, are in good agreement with our results. Extending the comparison to other existing experimental data, we see that in general the agreement is excellent for uranium with one exception concerning the energy of the M_3-N_4 transition quoted by Nordling and Hagström [38]. In the case of thorium, an overall agreement is also found especially with the results given by Nordling and Hagström but two strong discrepancies are found for the energies quoted by Bearden for the M_3-O_1 and M_3-O_4 lines. The latter are probably wrong since our energies are almost consistent with the XPS result from Ref. [32] and [34] and with the theoretical values of Larkins.

C. Level widths of subshells L_1 to N_5

The natural width of an x-ray line represents the sum of the widths of the two atomic levels participating in the transition. As a consequence one can build from the linewidths of the measured L and M x-ray lines a set of n simultaneous equations with m level widths as unknowns. If n > m as in our case, the set of equations can be solved by means of a least-squares method. However, because most transitions from the outer O and P shells are influenced by nonlifetime broadening effects, only those transitions that involve the L_1 to N_7 subshells should enter the set of equations.

The widths of the N_6 and N_7 levels are expected to be nearly equal [39] and small

TABLE VII. Atomic level widths in (eV) of subshells L_1 to N_5 of thorium. Our experimental results are compared with theoretical predictions from McGuire [21-23], Chen *et al.* [41,42], semi-empirical data from Krause and Oliver [26] and with fitted data of Campbell and Papp [39].

Subshell	This work	Refs. [21-23]	Refs. [41,42]	Ref. [26]	Ref. [39]
L_1	14.3 ± 0.2	20.4	15.8	13.7	14.7
L_2	8.5 ± 0.1	11.3	7.7	8.2	8.0
L_3	8.4 ± 0.1	7.0	7.7	7.1	7.5
M_1	14.6 ± 0.2	22.7	19.3		18.4
M_2	13.2 ± 0.2	15.5	14.5		14.3
M_3	7.9 ± 0.2	12.9	10.1		7.7
M_4	3.3 ± 0.1	3.2			3.3
M_5	3.4 ± 0.1	2.9			3.2
N_1	10.9 ± 0.1	11.2			11.1
N_2	9.0 ± 0.2	8.3			8.9
N_3	8.4 ± 0.2	7.5			7.5
N_4	4.5 ± 0.1	5.3			4.1
N_5	4.1 ± 0.1	5.3			4.1

(about 0.3 eV for uranium according to Ref. [36]). Thus, they cannot be extracted in a reliable way from M-$N_{6,7}$ and L-$N_{6,7}$ x-ray lines whose linewidths are 10-30 times bigger. For this reason the $N_{6,7}$ level widths of thorium and uranium were fixed at 0.15 eV and 0.29 eV, respectively, in the least-squares method. These values were taken from McGuire [23]. They were preferred to the XPS widths from Fuggle and Alvarado [40] because the latter, which are about 0.4 eV larger, are most likely affected by exchange splitting. Furthermore, as noticed by Campbell and Papp [39], calculations based on the single-particle model (SPM) as those of McGuire reproduce well the experimental N_7 level width in the region $70 \leq Z \leq 83$. Such SPM predictions should thus also valid for $Z > 83$.

For uranium we have used the L x-ray linewidths reported by Hoszowska *et al.* [11], except for the L_3-M_4, L_3-M_5 and L_3-N_5 transitions whose widths were taken from the experimental data of Amorim [25]. Amorim *et al.*'s results are indeed closer to the least-squares-fit to existing experimental data of Campbell and Papp [39] than those of Hoszowska *et al.* for these specific transitions.

If one restricts the least-squares method to the transitions involving the L_1 to N_7 levels, the M_3 subshell width enters the set of equations only via the L_1-M_3 and M_3-N_5 transitions. In the first transition, however, the linewidth is due mainly to the broad L_1 level and the corresponding equation is thus not very sensitive to the M_3 level width. Regarding the second transition, the experimental uncertainty on the linewidth (0.6 eV) is relatively large so that the influence of this line on the M_3 level width determined by the weighted least-squares-fit is also only moderate. For these reasons we have added in the sets of equations corresponding to thorium and uranium the M_3-O_5 transitions, taking for the O_5 level width the XPS values (0.6 ± 0.2 eV for thorium and

TABLE VIII. Atomic level widths in (eV) of subshells L_1 to N_5 of uranium. Our experimental results are compared with theoretical predictions from McGuire [21-23, 37], Chen *et al.* [41-43], semi-empirical data from Krause and Oliver [26] and with fitted data of Campbell and Papp [39].

Subshell	This work	Refs. [23,37]	Refs. [41-43]	Ref. [26]	Ref. [39]
L_1	16.0 ± 0.2	19.3	16.5	14.0	15.5
L_2	10.0 ± 0.1	10.9	8.6	9.3	9.3
L_3	8.4 ± 0.2	7.3	8.2	7.4	7.9
M_1	15.5 ± 0.2	23.0	19.5		18.5
M_2	14.1 ± 0.2	20.2	14.7		15.0
M_3	7.9 ± 0.2	12.6	10.4		7.5
M_4	3.2 ± 0.1	4.5	3.7		3.5
M_5	3.3 ± 0.1	4.2	3.6		3.5
N_1	12.6 ± 0.2	11.8			11.5
N_2	9.7 ± 0.2	7.5			9.5
N_3	8.7 ± 0.2	6.6			8.1
N_4	4.7 ± 0.1	4.2			4.2
N_5	4.2 ± 0.6	4.2			4.2

1.1 ± 0.3 eV for uranium) reported by Fuggle and Alvarado [40]. In this respect, it can be mentioned further that, in contrast to $O_{1\text{-}3}$ subshells, the O_5 level seems to be not affected by exchange splitting or solid state effects since no broadening nor asymmetry was observed in any of the *L* or *M* x-ray transitions from the O_5 level.

From the *L* and *M* x-ray linewidths determined in the present work and the ones discussed above two sets of 29 equations for thorium and 30 for uranium were obtained with 13 unknowns corresponding to the widths of the levels L_1 to N_5. The sets of simultaneous linear equations were solved by minimising the sums of the weighted squares of deviations. Weighting factors inversely proportional to the experimental errors and not to the squares of the latter were employed in order to give more consideration in the fit to the influence of weaker transitions. The so-obtained level widths are presented for thorium and uranium in Tables VII and VIII, respectively, where they are compared to results based on least-squares-fits to existing experimental data from Campbell and Papp [39] and to theoretical predictions from McGuire [21-23,37] and Chen [41-43]. The semi-empirical values reported by Krause and Oliver [26] for the subshells L_1 to L_3 are included in the tables.

In the careful and extensive compilation of existing experimental level widths reported by Campbell and Papp [39], most results are presented graphically and errors concerning their fits to available experimental data are in most cases not mentioned. However, if we assume an average relative uncertainty of about 5% for their results, one can see from Tables VII and VIII that our level widths are consistent with those of Campbell and Papp for all thorium and uranium subshells, except for the L_3 and M_1 subshells. Actually, the L_3 level width determined in our work seems to be too large by about 0.5-1.0 eV. This could indicate

that the nonlifetime broadening induced by the unresolved N satellites originating from L_jL_3N Coster-Kronig transitions is not as unimportant as anticipated. The larger discrepancy observed for the M_1 level width is more difficult to understand. The values deduced from our experiment are indeed 3.8 eV for thorium and 3.0 eV for uranium smaller than the fitted values from Campbell and Papp. One could argue that the discrepancy is due to the least-squares method itself because in the latter the determination of the M_1 level width is only anchored to the L_3-M_1 and L_2-M_1 transitions. This argument looks reasonable but, in our opinion, it does not completely clarify the question. The widths of the L_3-M_1 and L_2-M_1 transitions in thorium computed from the level widths quoted by Campbell and Papp are 25.9 and 26.4 eV, respectively, i.e., 2.3 and 3.3 eV larger than the values obtained in our study. This is intriguing because, on the one hand, the difference are more than ten times larger than the experimental errors and on the other hand because it is difficult to find plausible reasons explaining why observed spectral lines would be too narrow. A too large value of the instrumental broadening indeed cannot account for the observed differences because in that energy region the instrumental width is only 3.5 eV. Furthermore, if the M_1 widths are kept fixed in the least-squares method at the values quotes by Campbell and Papp, the widths given by the fit for the other levels are in poorer agreement than in case where the M_1 widths are used as free parameters. For all these reasons we are not convinced that the M_1 level widths of thorium and uranium obtained from our experiment are really too small.

The relative uncertainties estimated by Krause and Oliver [26] for their semi-empirical level widths are 20%, 10%, and 8%, respectively, for the L_1, L_2, and L_3 subshells. Comparing their values with our results, we observe again a good agreement for the L_1 and L_2 levels, whereas our L_3 level widths of thorium and uranium exceed Krause and Oliver data by 15% and 12%, respectively. Values from Campbell and Papp for the L_3 subshell are also bigger than those of Krause and Oliver, but they agree within the quoted uncertainty of 8%.

Larger discrepancies are observed when comparing our results to McGuire's predictions for the L [21,37], M [22,37] and N [23] level widths. Except for three levels of thorium (L_3, M_4, and M_5) and one of uranium (L_3), the predictions overestimate our results and those of Campbell and Papp for the L_1 to M_5 levels. The deviations are the largest for the L_1 and M_1 subshells where they reach about 40% indicating as already mentioned in Sec. IV A that McGuire's *LLX* and *MMX* Coster-Kronig yields are significantly overestimated. For the N_1 to N_5 levels, one observes an opposite trend of the theory which underestimates the experimental widths.

Relativistic independent particle calculations concerning atomic level widths were also performed by Chen *et al.*. For thorium results are only available for the L_1 to M_3 core levels [41,42]. For uranium predictions exists for the L_1 to M_5 subshells [41-43]. In Ref. [42] Chen *et al.* mention that their calculations overestimate the $M_{2,3}$ and M_1 Coster-Kronig rates in heavy atoms by ~10-15 % and ~30-50 %, respectively. This statement is confirmed by

TABLE IX. N_4 and N_5 level widths in (eV). Our experimentalresults are compared with theoretical predictions of Ohno and Wendin [44]. A1 approximation uses frozen-core potential and frozen Auger energy; A2 approximation uses frozen-core potential and relaxed and relativistic Auger energy.

	Thorium			Uranium		
		Theory			Theory	
Level	Present	A1	A2	Present	A1	A2
N_4	4.54 ± 0.13	4.63	3.49	4.70 ± 0.11	4.69	3.61
N_5	4.06 ± 0.13	4.63	3.90	4.15 ± 0.61	4.69	3.73

our results which show in addition that the overestimation is larger for the M_3 level than for the M_2 one. In general, however, the results of Chen *et al.* are noticeably closer to the experimental values than those of McGuire.

Finally, in Table IX the N_4 and N_5 level widths of thorium and uranium extracted from our measurements are compared to calculations performed by Ohno and Wendin [44] within the frame of a nonrelativistic many-body theory. The predictions were computed from two different approaches. In the so-called A1 approximation, a frozen-core potential and frozen Auger energy were used, while in the A2 approximation a frozen-core potential but relaxed and relativistic Auger energy were employed. From the comparison one sees that for both thorium and uranium our N_4 level widths are better reproduced by the A1 approximation, whereas for the N_5 subshell our experimental results are between the predictions corresponding to the two approximations. Ohno-Wendin calculations based on the same many-body model do also exist for the N_1, N_2 and N_3 level width. However, in the high-Z region, results are only available for mercury. These results were compared with XPS data from Svensson *et al.* [45]. A quite satisfactory agreement was found.

ACKNOWLEDGMENT

This work was partly supported by the Swiss National Science Foundation.

[1] M. Budnar and A. Mülheisen, Nucl. Instrum. Methods Phys. Res. B **75**, 81 (1993).

[2] J. A. Maxwell, W. J. Teesdale and J. L. Campbell, Nucl. Instrum. Methods Phys. Res. B **43**, 218 (1989).

[3] J. L. Campbell, Nucl. Instrum. Methods Phys. Res. B **49**, 115 (1990).

[4] T. Åberg, in *Atomic Inner-Shell Processes, edited by B. Crasemann (Academic Press, New-York, 1975), p353*.

[5] Ch. Herren and J.-Cl. Dousse, Phys. Rev. A **53**, 717 (1996).

[6] A. Mülheisen, M. Budnar and J.-Cl. Dousse, Phys. Rev. A **54**, 3852 (1996).

[7] Ch. Herren and J.-Cl. Dousse, Phys. Rev. A **56**, 2750 (1997).

[8] A. Mülheisen, M. Budnar and J.-Cl. Dousse, J. Hoszowska and Z. G. Zhao, X-Ray Spectrom. **27**, 337 (1998).

[9] J.-Cl. Dousse and J. Hoszowska, Phys. Rev. A **56**, 4517 (1997).

[10] T. Papp, J. L. Campbell, J. A. Maxwell, J.-X. Wang, W. J. Teesdale, Phys. Rev. A **45**, 1711 (1992).

[11] J. Hoszowska, J. Cl. Dousse and Ch. Rhême, Phys. Rev. A **50**, 123 (1994).

[12] B. Galley and J.-Cl. Dousse, Phys. Rev. A **50**, 3058 (1994).

[13] W. Beer, P. F. A. Goudsmit and L. Knecht, Nucl. Instrum. Methods Phys. Res. A **219**, 322 (1984).

[14] W. Schwitz, Nucl. Instrum. Methods **154**, 95 (1978).

[15] E. G. Kessler, Jr., R. D. Deslattes, D. Girard, W. Schwitz, L. Jacobs and O. Renner, Phys. Rev. A **26**, 2696 (1982).

[16] J. Hoszowska, J.-Cl. Dousse, J. Kern and Ch. Rhême, Nucl. Instrum. Methods Phys. Res. A **376**, 129 (1996).

[17] S. I. Salem and P. L. Lee, At. Data Nucl. Data Tables **18**, 223 (1976).

[18] J. A. Bearden, Rev. Mod. Phys. **39**, 78 (1967).

[19] F. James and M. Roos, Comput. Phys. Commun. **10**, 343 (1975).

[20] W. Uchai, C. W. Nestor, Jr., S. Raman, C. R. Vane, At. Data Nucl. Data Tables **34**, 201 (1986).

[21] E. J. McGuire, Phys. Rev. A **3**, 587 (1971).

[22] E. J. McGuire, Phys. Rev. A **5**, 1043 (1972).

[23] E. J. McGuire, Phys. Rev. A **9**, 1840 (1974).

[24] J. Merill and J. W. M. Dumond, Annals of Phys. **14**, 166 (1961).

[25] P. Amorim, L. Salgueiro, F. Parente and J. G. Ferreira, J. Phys. B **21**, 3851 (1988).

[26] M. O. Krause and J. H. Oliver, J. Phys. Chem. Ref. Data **8**, 328 (1979).

[27] F. Parente, M. H. Chen, B. Crasemann and H. Mark, At. Data Nucl. Data Tables **26**, 383 (1981).

[28] M. H. Chen, B. Crasemann and H. Mark, At. Data Nucl. Data Tables **24**, 13 (1979).

[29] F. Parente, M. L. Carvalho and L. Salgueiro. J. Phys. B: At. Mol. Phys. **16**, 4305 (1983).

[30] T. Åberg, Phys. Rev. A **156**, 35 (1967).

[31] T. A. Carlson and C. W. Nestor, Jr., Phys. Rev. A **8**, 2887 (1973).

[32] C. Nordling and S. Hagström, Z. Phys. **178**, 418 (1964).

[33] F. P. Larkins, At. Data Nucl. Data Tables **20**, 319 (1977).

[34] J. C. Fuggle and N. Mårtensson, J. Electron Spectrosc. Relat. Phenom. **21**, 275 (1980).

[35] C. Bonnelle and G. Lachère, J. Phys. (Paris) **35**, 295 (1974).

[36] O. Keski-Rahkonen, M. O. Krause, Phys. Rev. A **15**, 959 (1977).

[37] E. J. McGuire, in *Proceedings of the International Conference on Inner Shell Ionization Phenomena and Future Applications, Atlanta, Georgia, 1972,* edited by R. W. Flink, S. T. Manson, J. M. Palms, P. V. Rao, CONF-720404 (Natl. Tech. Information Service, U. S. Dept. of Commerce, Springfield, Va., 1973) p.662.

[38] C. Nordling and S. Hagström, Ark. Phys. **15**, 431 (1959).

[39] J. L. Campbell and T. Papp, X-ray Spectrom. **24**, 307 (1995).

[40] J. C. Fuggle and S. F. Alvarado, Phys. Rev. A **22**, 1615 (1980).

[41] M. H. Chen, B. Crasemann, and H. Mark, Phys. Rev. A **24**, 177 (1981).

[42] M. H. Chen, B. Crasemann, and H. Mark, Phys. Rev. A **27**, 2989 (1983).

[43] M. H. Chen, B. Crasemann, and H. Mark, Phys. Rev. A **21**, 449 (1980).

[44] M. Ohno and G. Wendin, Phys. Rev. A **31**, 2318 (1985).

[45] S. Svensson, N. Mårtensson, E. Basilier, P. Å. Malmquist, U. Gelius and K. Siegbahn, J. Electron Spectrosc. **9**, 51 (1976).

L_1 atomic level width of elements $62 \leq Z \leq 83$

P.-A. Raboud, M. Berset, J.-Cl. Dousse, and Y.-P. Maillard

Departement of Physics, University of Fribourg, Ch. du Musée 3, CH-1700 Fribourg, Switzerland

High-resolution measurements of the photoinduced dipole-forbidden L_1-$M_{4,5}$ x-ray emission lines were performed with a reflection-type and a transmission-type bent-crystal spectrometers for $_{62}$Sm, $_{67}$Ho, $_{70}$Yb, $_{74}$W, $_{78}$Pt, $_{80}$Hg, and $_{83}$Bi. From the observed linewidths of the L_1-$M_{4,5}$ x-ray transitions, the level widths of the subshell L_1 were determined assuming for the $M_{4,5}$ level widths the values reported recently by Campbell and Papp.

PACS number(s) : 32.70 Jz, 32.30 Rj, 32.80 Fb

I. INTRODUCTION

Precise and reliable data concerning atomic level widths are of interest in both theoretical and experimental physics. For theory such data are important because they can provide sensitive tests of atomic structure calculations. In particular, they permit to probe the goodness of theoretical predictions concerning total vacancy lifetimes, radiative and radiationless transition probabilities, or fluorescence yields. Atomic level widths and related x-ray linewidths are also of interest and value in high-resolution x-ray spectroscopy. Here a precise knowledge of x-ray linewidths is very helpful because it permits one to improve data analysis by diminishing the number of free fitting parameters and anchoring the natural linewidths of the observed transitions to known values. This in turn leads to a better accuracy in x-ray emission techniques such as high-resolution x-ray fluorescence and particle-induced x-ray emission. Furthermore, in a variety of experiments in which weak structures such as Radiative Auger Emission (RAE) lines or satellite x rays have to be extracted from the tails of close-lying and much more intense diagram transitions, the line shapes of the latter must be known accurately to obtain reliable results.

Several review papers dealing with atomic level widths can be found in the literature (see e.g. [1-3]). Most rely on theory and only a few of them on experimental data. More recently Campbell and Papp assembled a large set of measured level widths and x-ray linewidths, and derived an internally consistent set of level widths for the K shell to the N_7 subshell for all elements across the Periodic Table [4,5].

For the subshell L_1 ($2s_{1/2}$ atomic level) Campbell and Papp used results from XPS (X-ray Photoelectron Spectroscopy) measurements for the light elements and XES (X-ray Emission Spectroscopy) data for the elements pertaining to the region $40 \leq Z \leq 51$. To connect the latter data to recent XES results obtained for Th and U [6,7], they chose to

employ a set of L_1 Coster-Kronig and relative fluorescence yields of elements in the range $62 \leq Z \leq 79$ (Refs. [8-10]), assuming the radiative component of the L_1 widths, which was taken from [11]. The L_1 widths of Th and U were deduced by Campbell and Papp from the linewidths of the weak, dipole-forbidden L_1-M_4 and L_1-M_5 transitions observed in [6,7], assuming their recommended values for the M_4 and M_5 widths. The same references [6,7] provide also accurate linewidths for the stronger L_1-M_2, L_1-M_3, L_1-N_2 and L_1-N_3 lines but the latter were preferably employed as a source of the M_2, M_3, N_2 and N_3 widths assuming the L_1 widths derived with above mentioned method. The alternative of using in the region $62 < Z < 79$ old measurements [12] of the L_1-$N_{2,3}$ linewidths instead of the set of L_1 Coster-Kronig yields was also probed by Campbell and Papp. The obtained results were found to be 0.3-3.3 eV higher than the values derived from Coster-Kronig spectroscopy. In their determination of the recommended L_1 widths, Campbell and Papp renounced to use these XES data because of the age of the latter, their Z-dependence, and because of the 0.5-1.0 eV uncertainty in the $N_{2,3}$ widths. They pointed out, however, that there would be merit in remeasuring these L_1-$N_{2,3}$ transitions to ascertain if the trend determined from the Coster-Kronig spectroscopy data is indeed correct.

Following the suggestion of Campbell and Papp we have undertaken a series of high-resolution XES measurements in the Z-region of interest. Although dipole-forbidden L_1-$M_{4,5}$ transitions are very weak, they were preferred to the stronger L_1-$N_{2,3}$ transitions because the uncertainties of the recommended $M_{4,5}$ widths quoted in [5] are 2-10 times smaller than those of the $N_{2,3}$ widths and because it is not certain, in our opinion, that the many-body-effects which considerably enlarge the widths of the $N_{2,3}$ levels in the domain comprised between Sn and Ba are completely negligible for elements $Z > 56$. Actually non-lifetime broadening effects seem to have been observed for these levels up to Yb (Z=70) [13]. L_1-$M_{2,3}$ transitions could neither be employed because the single recent source of M_2 and M_3 level widths is the compilation by Campbell and Papp in which, the $M_{2,3}$ widths were already determined from L_1-$M_{2,3}$ transitions, assuming their recommended L_1 level widths. The quadrupole transitions L_1-$M_{4,5}$ of seven metallic elements in the range $62 \leq Z \leq 83$ were thus measured by means of high-resolution x-ray spectroscopy. From the observed linewidths, the level widths Γ_{L1} were determined assuming for $\Gamma_{M4,5}$ the recommended values of Campbell and Papp. Relative uncertainties varying between 4% (Bi) and 10% (Sm) were obtained for the so-derived L_1 level widths. Hence, a significant improvement of the existing Γ_{L1} data base is given by the present study since the errors quoted in [5] for the same elements are 16% and 55%, respectively. A spinoff result of our experiment is a set of accurate experimental energies for the weak L_1-M_4 and L_1-M_5 transitions.

II. EXPERIMENT

The measurements were performed at the University of Fribourg by means of two differents curved crystal spectrometers. For the

elements $_{78}$Pt, $_{80}$Hg, and $_{83}$Bi a Dumond transmission-type crystal spectrometer was employed. As this instrument cannot be used for photon energies below 10 keV, the L_1- M_4 and L_1- M_5 emission lines of the elements $_{62}$Sm, $_{67}$Ho, $_{70}$Yb, and $_{74}$W were measured with a von Hamos reflection-type crystal spectrometer.

Except for Hg, the targets consisted of 25 mm high × 5 mm wide metallic foils of natural Bi, Pt, W, Yb, Ho and Sm. The specified purity of the foils ranged between 99.9% and 99.97%. Due to the method of production the Ho foil contained about 1% Ta. Bismuth being a brittle metal, the thin Bi foil was mounted on a permanent polyester support. Sample thickness (15-22 mg/cm^2) were chosen to obtain about 95% of the maximum possible yield. The liquid Hg was enclosed in a 30 × 8 × 2 mm^3 stainless steel reservoir whose front wall was made of a 8 μm thick Kapton foil. The small cell was oriented so that the angle between the normal to the Kapton window and the target-to –crystal direction was 45 deg.

A. Measurements of elements $78 \leq Z \leq 83$

A detailed description of a similar transmission-type bent crystal spectrometer installed by the Fribourg group at the Paul Scherrer Institute (PSI) in Villigen, Switzerland, can be found in [14]. The instrument was operated in a so-called modified Dumond slit geometry [14]. In this geometry the target is viewed by the bent crystal through a narrow slit located on the focal circle. The 0.1-mm-wide vertical rectangular slit was made of two 5-mm-thick juxtaposed Pb plates. The target L x-ray emission was induced by means of a commercial 3 kW Coolidge-type x-ray tube with a Cr anode and a 0.5-mm thick window of nonporous beryllium. For the three targets the tube was operated at 80 kV and 35 mA. It was oriented so that the ionizing radiation was perpendicular to the target-crystal direction.

For the diffraction of the x rays the (110) reflecting planes of a 10×10-cm^2 quartz-crystal plate, 0.5 mm thick, were used. The quartz lamina was bent to a radius R = 313.5 cm by means of a bending device similar to the one described in Ref. [15]. The effective reflecting area of the crystal was 12 cm^2. The Bragg angles, i.e., the angles between the incident x-ray radiation and the reflecting planes of the crystal were approximately 10.6 deg., 11.6 deg. and 12.4 deg. for the Bi, Hg and Pt targets, respectively. They were measured by means of an optical laser interferometer with a precision of 3-5 × 10^{-3} arsec [16].

The x-ray detector was a 5-in.-diam. two component Phoswich scintillation counter, consisting of a thin (0.25 in.) NaI(Tl) crystal followed by an optically coupled thick (2 in.) CsI(Tl) crystal. Both crystals were mounted on the same photomultiplier tube. As the rising time of the signal is different for the two crystals, the events corresponding to each scintillation can be identified by pulse shape analysis [17]. This type of detector strongly reduces the Compton noise arising from high-energy photons [7,18]. A further reduction of the background was achieved by enclosing the Phoswich detector in heavy Pb-Cu-Al shielding, and by sorting on line the events of interest as a function of their energy. In order to reduce the absorption of the x rays in air,

evacuated tubes were mounted between the target and the crystal and between the crystal and the 66-cm-long Soller-slit collimator.

In the DuMond geometry, the measurements are carried out in a point-by-point way. As a result of the poor intensity of the L_1-$M_{4,5}$ transitions, very long acquisition times per point were needed. In order to minimize systematic errors related to long-term instabilities of the experimental set-up (e.g. fluctuations in the x-ray tube intensity), each spectrum was measured in many (30-40) successive scans which were then summed off-line.

The energy calibration of angular spectra observed with the DuMond spectrometer requires the crystal lattice-spacing and the zero of the Bragg angle scale of the spectrometer to be accurately known. The lattice-spacing of the SiO_2 (110) crystal employed in the present experiment was determined by measuring the $K\alpha_1$ transition of Au. The line was observed in 4^{th} order of reflection and on both sides of reflection. Using the so-determined double Bragg angle $2\theta_B$ and the energy of the Au $K\alpha_1$ transition (68804.94 ± 0.18 eV) quoted in [19], the value 2.456642(20) Å was obtained for the crystal lattice-spacing. In the Dumond geometry the so-called focussing distance i.e. the crystal-to-slit distance corresponding to the best instrumental resolution varies as a function of the photon energy. The L_1-$M_{4,5}$ measurements were thus performed at different focussing distances so that a new determination of the zero Bragg angle was necessary for each target. Because of the poor intensity of the L_1-$M_{4,5}$ transitions, stronger x-ray lines measured on both sides of reflection were employed for the determination of the different zero Bragg angles. These x-ray lines (Se $K\alpha_1$ and the Hg $L\gamma_1$ in 1^{st} order of reflection for the Pt and Hg measurements, and Te $K\alpha_1$ in 2^{nd} order of reflection for the Bi measurements) were chosen because they could be measured at about the same Bragg angle i.e. at the same focussing distance as the L_1-$M_{4,5}$ transitions.

The instrumental response of the DuMond spectrometer can be well reproduced by a Gaussian function whose standard deviation σ depends mainly on the crystal quality, precision of the crystal curvature and slit width. In first approximation, the angular instrumental broadening does not depend on the Bragg angle, provided that the above-mentioned focussing distance is adjusted to correspond to the central Bragg angle of the measured spectrum. In other words, neglecting the contribution of the Darwin width which is only a fraction of arcsec in our case, the angular resolution of the spectrometer can be considered as being the same for photons of different energies or photons diffracted in different orders of reflection. We took advantage of this property to determine the angular instrumental broadening of the spectrometer. The latter was indeed derived from the $K\alpha_1$ transition of Sn measured in 1^{st}, 2^{nd} and 3^{rd} orders of reflection. From these measurements, we obtained a set of 3 equations with 2 unknowns, the angular instrumental broadening σ and the natural linewidth of the Sn $K\alpha_1$ transition Γ. Solving this set of equations by means of a non-linear least-squares-fit method, we obtained $\sigma = 5.21 \pm 0.10$ arcsec and as a spinoff result,

$\Gamma = 11.04 \pm 0.11$ eV. The latter result was found to be in good agreement with the value of 10.96 ± 0.38 eV derived from [5]. The obtained angular broadening of the spectrometer of 5.21 arcsec corresponded to FWHM instrumental resolutions of 3.2 eV, 3.6 eV and 4.4 eV, respectively, for the Pt, Hg and Bi L_1-$M_{4,5}$ x-ray spectra.

B. Measurements of elements $62 \leq Z \leq 74$

The von Hamos curved crystal facility is described in details in [20]. The principal elements of this instrument are an x-ray source defined by a rectangular slit, a cylindrically bent crystal and a position sensitive detector. In the von Hamos geometry the crystal is bent around an axis which is parallel to the direction of dispersion and provides focusing in the nondispersive direction. For a fixed position of the components, the impact coordinate on the detector of a reflected x-ray corresponds geometrically to a particular Bragg angle and hence to a particular photon energy. In contrast to the DuMond geometry, the von Hamos geometry permits thus at one position of the spectrometer components data collection over an energy bandwidth which is limited by the detector length. The vertical rectangular slit consisted of two juxtaposed Ta pieces 0.3 mm thick and 10 mm high. The slit width was 0.1 mm for all measurements. The target L x-ray emission was also induced by means of a Cr anode x-ray tube. The latter was operated, however, at lower HV values (typically 60 kV 45mA).

Emitted photons were reflected in the first order by the $(2\bar{2}3)$ reflecting planes of a quartz crystal. The curvature radius of the 5-cm-wide and 10-cm-high crystal was 25.4 cm. Reflected photons were detected by a 27.6-mm-long and 6.9-mm-high deep-depleted (50 μm) CCD (charged coupled device) position-sensitive detector. The latter which consisted of 1024 pixels in the horizontal direction of dispersion × 256 pixels in the vertical direction, with a pixel resolution of 27 μm, was thermoelectrically cooled to –60 °C. The diffracted x rays hitting the CCD built a two-dimensional pattern on the detector. Each measurement consisted in collecting several thousands of two-dimensional images. For each image, good event pixels were sorted by setting a energy window corresponding to the x rays of interest. This permitted us to reject background events and higher-order reflections. Without this sorting process, it would have been almost impossible to resolve the extremely weak L_1-$M_{4,5}$ transitions. The filtered images were then added and their sum projected on the horizontal axis to obtain the final energy spectrum.

The energy calibration and the determination of the instrumental response of the von Hamos spectrometer were performed by measuring the $K\alpha_1$ x-ray lines of several elements ranging between $26 \leq Z \leq 33$. It was found that for this energy range (6404-10544 eV) the instrumental response of the spectrometer could be well reproduced by a Gaussian profile whose standard deviation σ varied as a function of the x-ray energy between 1.44 and 1.78 eV. The natural linewidths and energies of the $K\alpha_1$ transitions were taken from Ref. [5] and Ref. [21], respectively.

III. DATA ANALYSIS

The L_1-$M_{4,5}$ x-ray spectra observed with the DuMond and the von Hamos spectrometers were analyzed by means of the least-squares-fitting computer code Minuit [22], employing Voigtian profiles to reproduce the observed x-ray lines. Voigtian functions were used because they correspond to the convolution of the Gaussian instrumental broadening with the Lorentzian representing the natural line shape of an x-ray transition. The natural widths of the x-ray lines of interest were extracted by keeping fixed in the fit the known Gaussian experimental broadening. The energies and the intensities of the transitions as well as a linear background were used as additional free fitting parameters. The fitted spectra are presented in Figs. 1 and 2.

At first glance, one sees that, as expected, the measured transitions are very weak, the net intensity at the top of the L_1-M_5 transitions varying from 0.07 s^{-1} for Bi (Fig. 1(a)) down to 0.003 s^{-1} for Sm (Fig. 2(d)). These weak intensities originate from the poor x-ray emission rates of the L_1-$M_{4,5}$ transitions (for Sm, the yield ratio $I_{L_1-M_5} \div I_{K-L_3}$ quoted by Scofield [23] is only 3×10^{-4}!) and from the small efficiency of crystal spectrometers. This small efficiency which is due mainly to the small solid angle sustented by crystal spectrometers (about 10^{-5} steradian for both instruments in our case) is the price to pay to obtain instrumental resolutions in the eV range. The measured yield ratios $I_{L_1-M_4} \div I_{L_1-M_5}$ were found to slightly decrease with Z, varying from 0.72 for Sm down to 0.62 for Bi. In this Z-region, Scofield's calculations predict for this ratio a constant value of 0.67 [23]. In case of Yb, the fitted ratio is bigger than one (1.08). This is due to the L_3 absorption edge which is located at 8944 eV i.e. between the L_1-M_4 and L_1-M_5 transitions.

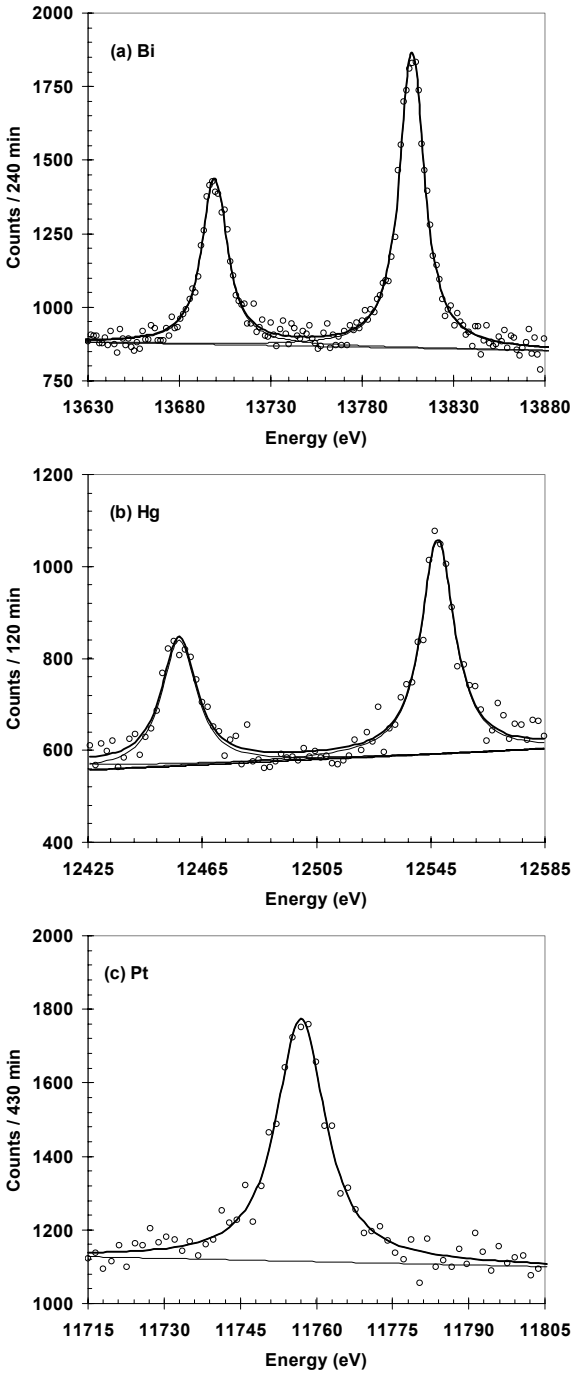

FIG. 1. High-resolution L_1-$M_{4,5}$ emission spectra measured with the DuMond transmission-type crystal spectrometer. For Pt only the L_1-M_5 was measured.

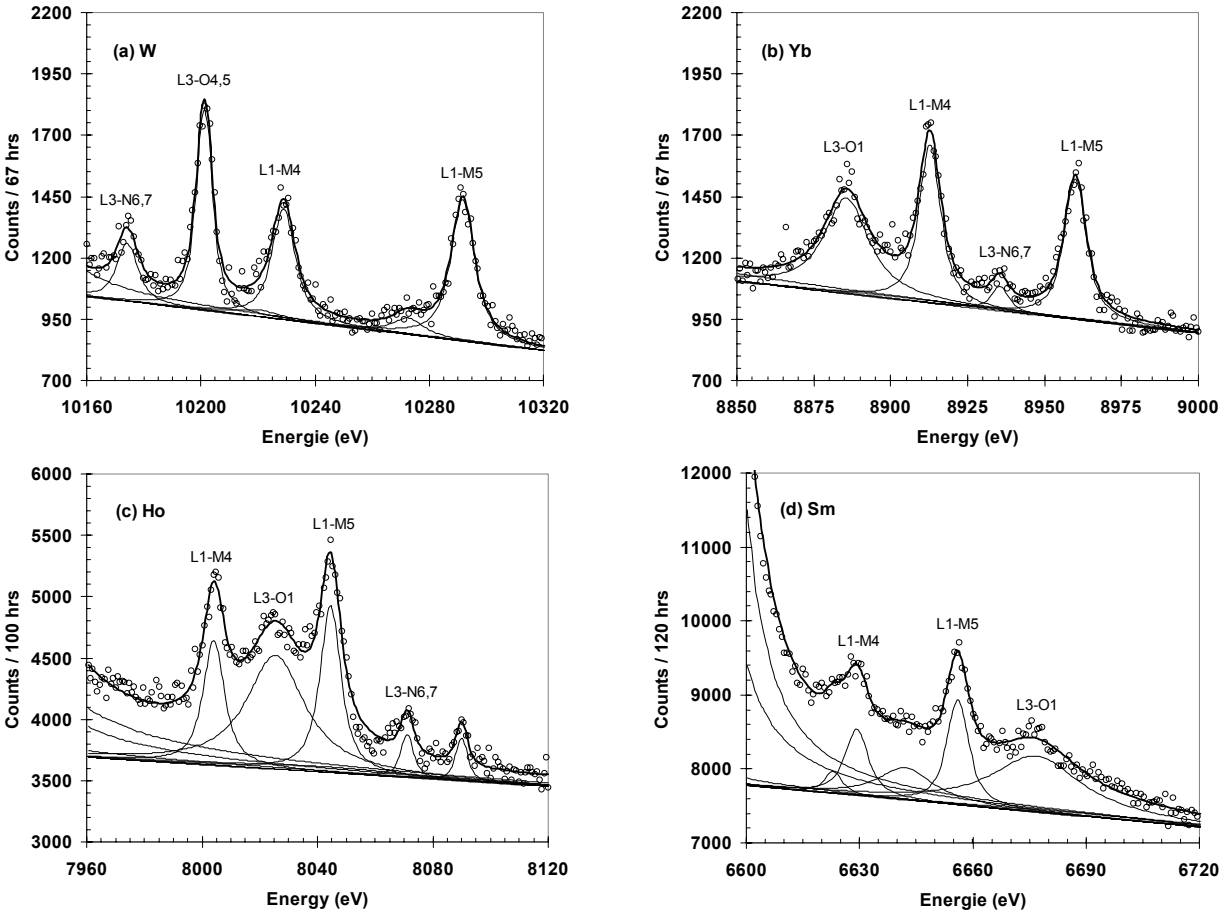

FIG. 2. High-resolution L x-ray emission spectra measured with the von Hamos reflection-type crystal spectrometer. The lines observed at 10275 eV in the W spectrum and at 8086 eV in the Ho spectrum correspond to the Re $L\beta_2$ and Ta $L\alpha_2$ transitions from trace impurities in the targets and anode of the x-ray tube. In the Sm spectrum the broad line at about 6640 eV corresponds to the M-satellite of the L_3-$N_{4,5}$ transition, whereas the excess of intensity occuring at 6623 eV could not be indentified clearly. The intensity increases appearing on the low-energy sides of the Ho and Sm spectra are due to the tails of the strong L_3-$N_{4,5}$ transitions.

For transmission-type spectrometers, an additional factor that contributes to diminish the luminosity of the instrument is the x-ray absorption by the crystal lamina. For Pt, the lightest element that could be measured with the DuMond spectrometer, about 80% of the L_1-$M_{4,5}$ x rays were absorbed in the 0.5 mm thick quartz crystal so that about 16 days were needed to scan the single L_1-M_5 transition (Fig. 1(c)). Thus, for this element, we renounced to measure the even weaker L_1-M_4 transition. Nevertheless, as shown in Fig. 1, in spite of this crystal absorption problem, clean data were obtain with the DuMond spectrometer. In the three spectra the lines of interest could be indeed clearly resolved from the relatively flat background and no particular problem was encountered during the analysis which led to precise and reliable results.

For the lower-Z elements observed with the von Hamos spectrometer, the measurements and data analysis were complicated with the presence of several L_3 x rays in the vicinity of the L_1-$M_{4,5}$ lines of interest, namely the L_3-$N_{6,7}$ and L_3-$O_{4,5}$ lines in the W spectrum (Fig. 2(a)), the L_3-O_1 and L_3-$N_{6,7}$ lines in the Yb and Ho spectra (Figs. 2(b) and 2(c)) and the L_3-O_1 line

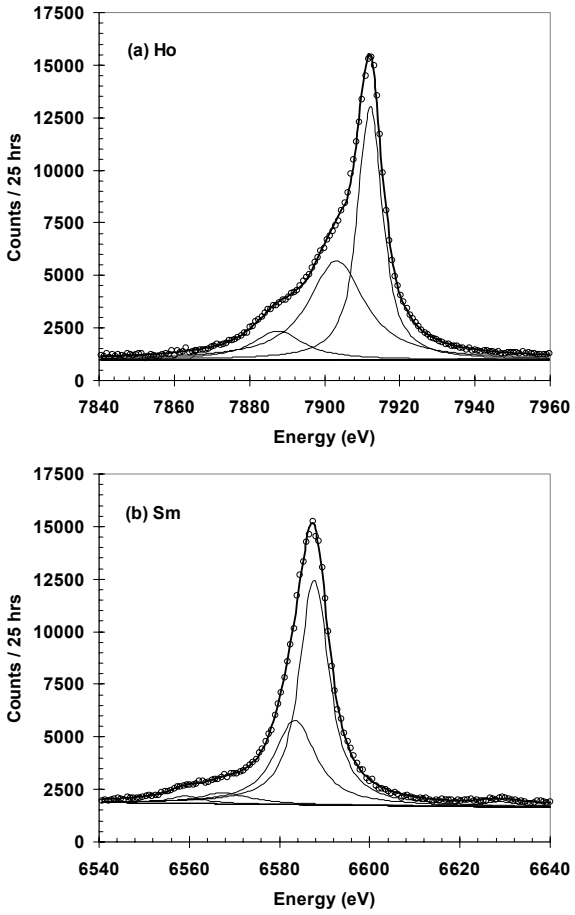

FIG. 3. High-resolution x-ray spectra of the $L\beta_{2,15}$ transitions of (a) holmium and (b) samarium.

in the Sm spectrum (Fig. 2(d)). Some characteristic x-ray lines from trace impurities in the targets or anode of the x-ray tube were also observed in the W, Ho and Sm spectra at energies of 10275 eV, 8086 eV and 6623 eV, respectively. Whereas a clear assignment was found for the first two lines (Re $L\beta_2$ and Ta $L\alpha_2$), the third one could not be identified undoubtedly. Furthermore, for Ho and especially Sm, the L_1-$M_{4,5}$ lines are sitting on the high-energy tail of the strong close-lying $L\beta_{2,15}$ doublet (L_3-$N_{4,5}$ transition). As fitted values of the linewidth and intensity of the L_1-$M_{4,5}$ x-ray lines were found to be sensitive to the shape of the $L\beta_{2,15}$ tails, high-resolution measurements of the L_3-$N_{4,5}$ transition were performed for Ho and Sm. Results of these complementary measurements are shown in Fig. 3. One sees that for both targets the $L\beta_{2,15}$ lines are broad and evince strong asymmetries on their low-energy flank. This non-lifetime broadening is characteristic of rare-earth elements. It has been already observed [24,25] and explained in terms of multiplet splitting of the $4d_{3/2}$ and $4d_{5/2}$ orbitals as a result of exchange interactions between $4f$ and $4d$ electrons. In the fitting procedure, the asymmetric profiles of the Ho and Sm L_3-$N_{4,5}$ transitions could be well reproduced by the sum of respectively three and four Voigtians, whose position, Lorentzian width and relative intensity were used as free fitting parameters. These parameters were then kept fixed at the obtained values in the analysis of the L_1-$M_{4,5}$ spectra, except the intensity of the strongest Voigtian which was let free and served thus as a scaling factor.

A further complication encountered in the analysis of the spectra measured with the von Hamos spectrometer arose from satellite x-ray lines. Indeed, as a result of L_iL_jN and L_iL_jM Coster-Kronig transitions, L_2 and L_3 fluorescence x rays may present on their high-energy side N- and M-satellite structures of significant intensities. In general, the energy shifts of satellites relative to the parent diagram lines increase with the principal quantum number of the transition electron and decrease with the principal quantum number of the spectator vacancy. As a result, for L x rays, M-satellites can be well resolved whereas N-satellites are poorly separated from the diagram lines and occur only as asymmetries on the high-energy flank of the latter, except

for transitions from the outer subshells O_i for which a better separation is observed. In addition, as the spectator vacancies can be located in different subshells and many couplings between the two holes are possible in the initial and final states, satellite lines consist of numerous components that vary in energy and intensity. Profiles of satellite x-ray lines are thus broad and the probability for satellites to overlap with other diagram lines is not negligible in *L* x-ray spectra. In measurements employing x-ray tubes for the production of the target fluorescence x-ray emission, double $L^{-1}N^{-1}$ or $L^{-1}M^{-1}$ hole-states can also be induced by *KLN* or *KLM* Auger transitions, provided that the high-voltage of the x-ray lamp is markedly bigger than the 1*s* binding energy of the irradiated target element. *KLM* Auger yields being smaller than *LLM* Coster-Kronig yields, only *M*-satellite structures related to strong *L* diagram lines have, however, to be considered in this case. For W, Yb, Ho and Sm, L_iL_jM Coster-Kronig transitions are energetically forbidden and only the *K*-shell binding energy of Sm (48.6 keV) is significantly smaller than the high-voltage value (60 kV) at which the x-ray tube was operated. For this reason, the L_1-$M_{4,5}$ spectrum of Sm is the single one that might be affected by *M*-satellites. Actually, the excess of intensity observed between the L_1-M_4 and L_1-M_5 lines (Fig. 2(d)) is due to the $L_3^{-1}M^{-1}$-$N_{4,5}^{-1}M^{-1}$ satellite transition. The latter was fitted with a single Lorentzian whose energy, width and intensity were let free in the analysis. An energy shift of about 54 eV was obtained from the fit. This result was compared to values derived from the data quoted in [26,27]. A satisfactory agreement in the order of a few eV was found.

N-satellites of the L_3-$O_{4,5}$ (W) and L_3-O_1 (Yb, Ho and Sm) transitions were also included in the data analysis. As shown in Fig. 2(a), the *N*-satellite (at about 10220 eV) of the W L_3-$O_{4,5}$ transition is overlapping with the L_1-M_4 line. Any attempt to let free in the fit the satellite parameters failed so that the energy , Lorentzian width and relative intensity of this satellite had to be kept at fixed values. The latter, however, could not be derived from Ref. [26] in which *L*-*O* transitions are not considered, neither from [27] which gives results for *M*-satellites only. The difficulty was circumvented by measuring the L_3-$O_{4,5}$ transition of Hg with the DuMond spectrometer. Mercury was chosen because the $L_3^{-1}N^{-1}$-$O_{4,5}^{-1}N^{-1}$ satellite of this element was found to be well resolved from the diagram line and not overlapping with any other transition. The values obtained from the fit for the energy shift ΔE, width Γ_{sat} and relative intensity $I_{sat} \div I_{diagr}$ of the Hg satellite were then employed to determine the unknown W *N*-satellite parameters. The dependence of the satellite parameters on the atomic number *Z* of the target-element was taken into account by means of the following relations:

$$\Delta E(Z) = \Delta E(Z = 80)(1 + \alpha(Z - 80)) \quad [1]$$

$$\frac{\Gamma_{sat}}{\Gamma_{diagr}}(Z) = \frac{\Gamma_{sat}}{\Gamma_{diagr}}(Z = 80)(1 + \alpha(Z - 80)) \quad [2]$$

$$\frac{I_{sat}}{I_{diagr}}(Z) = \frac{I_{sat}}{I_{diagr}}(Z = 80)\frac{\sum \Gamma_{LLN}(Z)}{\sum \Gamma_{LLN}(Z = 80)} \quad [3]$$

The *Z*-scaling factor α was deduced from the plots given in Ref. [27] for *M*-satellites of L_1-$O_{2,3}$ transitions, assuming thus a similar

TABLE I. Energies in (eV) of the measured L_1-$M_{4,5}$ x-ray emission lines. Present results are compared to Bearden & Burr's [31] and Storm & Israel's [32] data.

Z	L_1-M_4					L_1-M_5				
	Energy	Error		Ref. [31]	Ref. [32]	Energy	Error		Ref. [31]	Ref. [32]
		Fit	Total				Fit	Total		
$_{62}$Sm	6628.75[a]	0.21	0.26	6630.8(1.3)	6630	6655.66[a]	0.13	0.14	6656.6(1.2)	6658
$_{67}$Ho	8004.18[b]	0.14	0.15	8002.7(1.2)	8002	8044.71[b]	0.13	0.14	8042.8(1.3)	8043
$_{70}$Yb	8913.22[c]	0.12	0.14	8910.1(9)	8912	8960.55[c]	0.18	0.19	8958.6(9)	8961
$_{74}$W	10228.86[d]	0.20	0.24	10228.6(6)	10227	10291.71[d]	0.17	0.22	10290.6(6)	10289
$_{78}$Pt						11756.87[e]	0.20	0.22	11758.3(7)	11758
$_{80}$Hg	12457.05[e]	0.51	0.52	12454.4(1.5)	12457	12547.60[e]	0.26	0.29	12544.4(1.5)	12547
$_{83}$Bi	13698.96[e]	0.30	0.32	13699.7(7)	13702	13806.91[e]	0.16	0.20	13807.9(7)	13810

[a] Reference energy: 6930.44(5) eV (Co $K\alpha_1$)
[b] Reference energy: 8047.92(2) eV (Cu $K\alpha_1$)
[c] Reference energy: 8639.01(6) eV (Zn $K\alpha_1$)
[d] Reference energy: 10543.86(13) eV (As $K\alpha_1$)
[e] Reference energy: 68804.94(18) eV (Au $K\alpha_1$ n=4)

dependence on Z for N- and M-satellites. The transition widths Γ_{diagr} were derived from the level widths quoted in [5] and the Coster-Kronig yields Γ_{LLN} were taken from [28]. The same method was then employed to determine the N-satellite parameters of the transitions L_3-O_1.The crudity of these approximations was taken into consideration by assuming relative uncertainties of 20% for the so-determined N-satellite parameters.

IV. RESULTS AND DISCUSSION

A. Energies

The energies of the measured L_1-$M_{4,5}$ transitions are given in Table I. For Pt, Hg and Bi our results are based on the energy of the Au $K\alpha_1$ transition which was determined by Kessler *et al*. with a precision of 2.6 ppm [19]. The uncertainties quoted for these three elements reflect mainly the statistical errors given by the fitting procedure. Uncertainties that originate from the crystal lattice-spacing and from the determination of the zero Bragg angles are included in the indicated total errors. For Sm, Ho, Yb and W, our values were determined from the $K\alpha_1$ wavelengths of Co, Cu, Zn and As listed in the table of Bearden [21]. Since the latter values are given in the Å* scale, they were corrected by the conversion factor 1.0000167 Å/Å* [29] and then converted to energies using the energy-wavelength product V·λ=12398.520 eV·Å [30]. The uncertainties quoted by Bearden [21] being probable errors (50% confidence limits), they were expanded by 1.48 to obtain standard deviation errors (67% confidence limits). The so-determined reference energies and associated errors are given as footnotes in Table I. Here again, statistical errors represent the principal source of uncertainty. The sensitivity of the L_1-$M_{4,5}$ transition energies to the fitted satellite structures was probed. The corresponding uncertainties were considered in the error budget. Further sources of uncertainties inherent to the von Hamos

TABLE II: Natural linewidths in (eV) of the measured L_1-$M_{4,5}$ x-ray emission lines.

Z	L_1-M_4			L_1-M_5		
	Linewidth	Error		Linewidth	Error	
		Fit	Total		Fit	Total
$_{62}$Sm	5.94	0.68	0.76	5.53	0.56	0.62
$_{67}$Ho	7.45	0.60	0.61	7.31	0.42	0.44
$_{70}$Yb	6.60	0.38	0.40	6.91	0.38	0.40
$_{74}$W	7.96	0.60	0.65	8.21	0.50	0.52
$_{78}$Pt				10.63	0.66	0.66
$_{80}$Hg	13.39	1.39	1.39	12.75	0.93	0.93
$_{83}$Bi	15.27	0.79	0.79	15.00	0.47	0.47

spectrometer such as the distance between the crystal and detector axes were also taken into account in the total errors.

To our knowledge there are no other high-resolution data concerning L_1-$M_{4,5}$ x rays in the domain $62 \leq Z \leq 83$. Hence, the present results were compared to values that were derived from the differences between the L_1 and M_4 or M_5 binding energies given by Bearden and Burr [31] and Storm and Israel [32]. From Table I one sees that deviations ranging from –3 eV to +3 eV are observed. One can also notice that most of the Bearden and Burr's data, for which the quoted probable errors were converted in Table I in 1-σ errors as discussed above, are inconsistent with our results. Because modern data concerning core-level energies for the elements investigated in the present study are scarce, we are embarrassed to discuss in details the observed deviations. However, in case of Sm, the single studied element for which we found more recent data for the $M_{4,5}$ binding energies [33], values of 1110.9 eV and 1083.4 eV are given, that are also in disagreement with the values of 1106.0 ± 0.8 eV and 1080.2 ± 0.6 eV quoted by Bearden and Burr. Furthermore, for the N subshells for which relatively modern information are available [34], similar deviations of 1-3 eV are observed relative to [31] for W, Pt, Hg and Bi. For the N_3 level of Hg, the deviation is even 5.6 eV i.e. four times larger than the probable error given by Bearden and Burr for this level.

To better probe the precision and reliability of our results, we also measured the L_1-N_3, M_4-N_6 and M_5-N_7 transitions of Hg. For the first transition which was observed with the DuMond spectrometer, an energy of 14266.16 ± 0.22 eV was obtained. By adding to the latter value the N_3 binding energy taken from [35] one finds a value of 14843.06 ± 0.30 eV for the binding energy of the L_1 level (the corresponding value quoted by Bearden and Burr is 14839.3 ± 1.0 eV). The M_4-N_6 and M_5-N_7 lines were measured with the von Hamos spectrometer. From the obtained transition energies (2282.25 ± 0.05 eV and 2195.57 ± 0.12 eV) and the $N_{6,7}$ binding energies given in [35], values of 2386.25 ± 0.11 eV and 2295.57 ± 0.16 eV were found for the binding energies of the M_4 and M_5 levels

(Bearden and Burr give values of 2384.9 ± 0.3 eV and 2294.9 ± 0.3 eV, respectively). The energies of the L_1-$M_{4,5}$ transitions derived from the so-determined L_1 and $M_{4,5}$ binding energies are thus 12456.81 ± 0.32 eV and 12547.49 ± 0.34 eV, values which are both in good agreement with the Hg results presented in Table I.

B. Linewidths

The fitted linewidths of the L_1-$M_{4,5}$ transitions and the corresponding uncertainties are presented in Table II. As for the energies, the principal contribution to the total error originates from the matrix error of the fitting procedure. This is not really surprising in view of the poor intensity of the L_1-$M_{4,5}$ transitions. For Pt, Hg and Bi, which were measured with the DuMond spectrometer, the natural linewidths are 3-4 times bigger than the instrumental broadening. As the latter could be determined with a precision of about 2%, the contribution of the instrumental response uncertainty to the total errors quoted in Table II is negligibly small.

As there is no existing information in the literature about measured linewidths of the weak L_1-$M_{4,5}$ transitions, we have compared our results to values derived from the sum of the L_1 and $M_{4,5}$ level widths quoted by Campbell and Papp [5]. The comparison showed that our data agree with the ones of Campbell and Papp within the total errors quoted in Table II, except for Ho and Sm for which a strong discrepancy is observed. For these two elements, our values are indeed about 1.6 eV bigger than those deduced from [5]. To better understand the origin of this

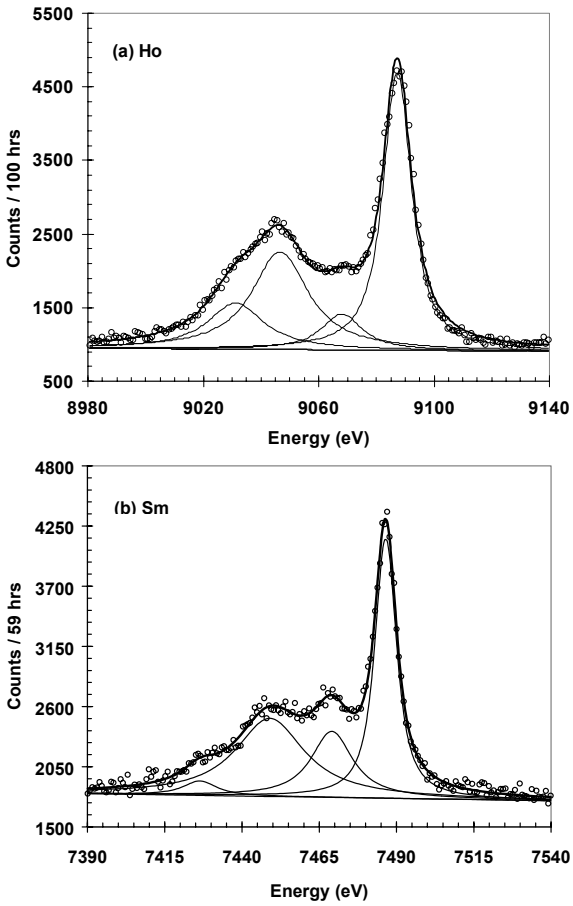

FIG. 4. High-resolution x-ray spectra of the $L\gamma_{2,3}$ transitions of (a) holmium and (b) samarium.

disagreement, the L_2-M_4, L_1-M_2 and L_1-$N_{2,3}$ transitions of Ho as well as the L_1-$N_{2,3}$ transition of Sm were measured with the von Hamos spectrometer.

The L_2-M_4, and L_1-M_2 transitions which are close in energy could be measured simultaneously, the two transitions being covered by a single CCD length. The analysis of these two lines did not give rise to any problem. The $L\gamma_{2,3}$ x-ray lines (L_1-$N_{2,3}$ transitions) of Ho and Sm are presented in Fig. 4. For both elements a complex spectral profile was observed. Similar lineshapes were obtained in XES measurements of rare-earth elements [36] and in 4*p* XPS measurements of elements ranging from $_{42}$Mo to $_{73}$Ta [13]. The

TABLE III. Atomic level widths in (eV) for the subshell L_1. Our experimental results are compared with the recommended values of Campbell and Papp [5] and theoretical predictions of Perkin *et al*. [11] and McGuire [37]

	Experimental		Theoretical		
Z	Present	Ref. [5]	Ref. [11]	Ref. [37]	
$_{62}$Sm	4.83 ± 0.49	3.3 ± 1.5	4.3		
$_{67}$Ho	6.23 ± 0.36	4.5 ± 1.5	5.0	5.1[a]	5.9[b]
$_{70}$Yb	5.40 ± 0.30	5.2 ± 1.5	8.0		
$_{74}$W	6.41 ± 0.43	6.3 ± 1.5	11.6	6.7[a]	7.8[b]
$_{78}$Pt	8.55 ± 0.69	8.8 ± 2.0	13.4		
$_{80}$Hg	10.67 ± 0.79	10.5 ± 2.0	13.8		
$_{83}$Bi	12.50 ± 0.45	12.3 ± 2.0	14.0	14.5[a]	19.3[b]

[a] Direct calculations
[b] Adjusted calculations

observed anomalous features of the spectra were explained by the strong configuration interaction between 4*p* single-hole states and 4*d* double-hole states resulting from $4p^{-1} - 4d^{-2}4(n,\varepsilon)4f^{n+1}$ super Coster-Kronig transitions. As shown in Fig. 4, the two complex $L\gamma_{2,3}$ profiles could be fitted with four juxtaposed Voigtians each. As reported in [38], for Sm, the main peak at 7486 eV should correspond to the well-defined relaxed core level of the $4p_{3/2}$ hole with more than half of the original strength peak of the $4p_{3/2}$ hole. Assuming the same interpretation for Ho, we also assigned the strongest Voigtian at 9087 eV to the L_1-N_3 transition.

For the L_2-M_4, transition of Ho, a linewidth of 5.34 ± 0.13 eV was obtained from the fit, in good agreement with the value of 5.22 ± 0.42 eV deduced from [5]. For the L_1-M_2 and L_1-N_3 transitions, however, linewidths of 13.84 ± 0.18 eV and 10.62 ± 0.13 eV were found, results which are both bigger than the values of 10.8 ± 1.7 eV and 7.5 ± 1.6 eV derived from [5]. For Sm , the same trend was observed, the measured L_1-N_3 linewidth (7.5 ± 0.18 eV) being bigger than the value (5.5 ± 1.6 eV) deduced from the Tables of Campbell and Papp. We are thus inclined to explain the discrepancies observed in the Ho and Sm transitions involving the L_1 subshell by a non-lifetime broadening of the 2*s* level. This effect will be discussed more in details in the next section.

C. Level widths

The L_1 level widths obtained in the present study are presented in Table III. They were determined from the weighted averages of the differences between the linewidths of the L_1-M_4 and L_1-M_5 transitions given in Table II and the recommended values of the $M_{4,5}$ level widths quoted by Campbell and Papp [5]. For Pt, the L_1 width was derived from the sole L_1-M_5 transition. The 10% uncertainties assumed in [5] for the $M_{4,5}$ level widths are included in the indicated errors. The latter vary from 4% for the heaviest measured element (Bi) up to 10% for the lightest one (Sm). Also

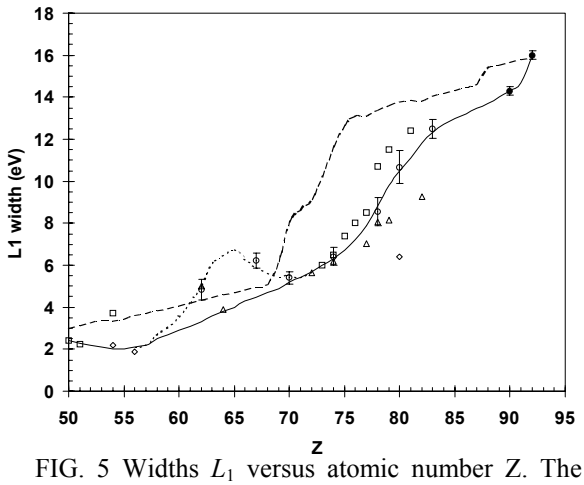

FIG. 5 Widths L_1 versus atomic number Z. The solid line represents the recommended values of Campbell and Papp [5], the dashed line results of independent-particle model calculations of Perkins *et al*. [11], and the dotted line predictions derived from the present work for rare-earth elements. Experimental data from different sources are also presented, using the following symbols: ◇ x-ray absorption edge results from Refs. [40,41], △ results derived from Coster-Kronig transition probabilities from Refs. [8-10], □ x-ray emission spectroscopy results from Refs. [12,39], ● x-ray emission spectroscopy results for thorium and uranium from Refs. [6,7], ○ present results.

reported in Table III are the L_1 level widths recommended by Campbell and Papp [5] with the corresponding errors and theoretical predictions based on the independent-particle model from two different sources. The first one is a work by Perkins *et al*. [11] whose results can be find in the LLNL (Lawrence Livermore National Laboratory) Evaluated Atomic Data Library (EADL). The second set of theoretical predictions is due to McGuire [37]. Here, however, results are available for Ho, W and Bi only. For the three targets two values are given, that correspond to results of either direct calculations or calculations in which some theoretical parameters were anchored on existing experimental data. Our results are also presented graphically in Fig. 5 which gives an overview of existing information about the level width of the subshell L_1 in the range $50 \leq Z \leq 92$.

As mentioned in the preceding section, an excellent agreement is found between our results and the values quoted in [5] for the elements $70 \leq Z \leq 83$, the average deviation (0.19 eV) being 3 times smaller than the average value of the quoted uncertainties (0.53 eV). In contrast to that, the results found for Ho and Sm are significantly bigger than the recommended values of Campbell and Papp. For Sm the deviation corresponds to about 3σ and for Ho even to 5σ, whereas for Yb, the third rare-earth element investigated in the present study, no discrepancy is observed. At this point, it is interesting to note that for Sm a result of 5.0 ± 0.6 eV, consistent with the value found in the present study, was obtained in a relatively recent Coster-Kronig measurement [8]. Some broadening of the L_1 subshell seems thus to affect Sm and Ho. Actually, a similar behaviour is observed for the 5*s* level, the linewidths of the L_3-O_1 transition being about 10 eV broader for Sm and Ho than for Yb. However, the O_1 subshell broadening, contrary to the L_1 one, is not new. Indeed, a multiplet splitting of the 4*s* and 5*s* levels of the rare-earth has been also observed in XPS measurements [42]. This splitting was explained to originate from energy difference between the *s*-electron spin-up and spin-down final states. We are inclined to believe that the broadening of the L_1 level observed for Sm and Ho but not for Yb arises from the same effect. Assuming that the exchange interaction of the 2*s* hole in the initial state is larger or similar to the *L*-*S* coupling energy of the 4*f* electrons, one can indeed consider the spin $s = ½$ of the 2*s*

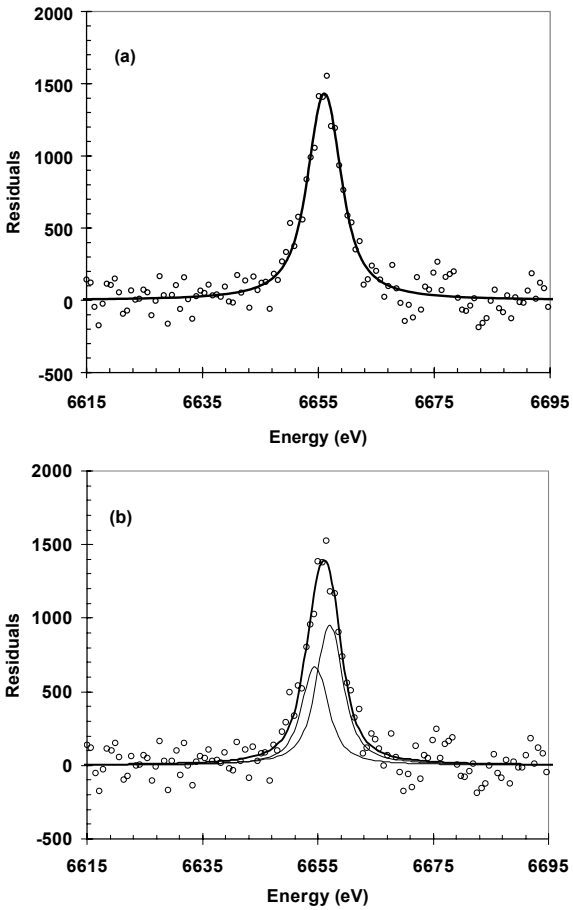

FIG. 6. One- and two-components fits of the residual L_1-M_5 x-ray spectrum of Sm.

subshell to couple with the spin S of the 4f subshell to yield the total spin $S' = S \pm ½$, so that the coupling results in a doublet. As the intensities of the two components of the doublet should be proportional to the respective multiplicities $(2S' + 1)(2L + 1)$, the yield ratio of the two components is given by:

$$\frac{I_1}{I_2} = \frac{(2(S+1/2)+1)(2L+1)}{(2(S-1/2)+1)(2L+1)} = \frac{S+1}{S} \quad (4)$$

where I_1 stands for the intensity of the higher-energy component. The splitting energy can be deduced from Hartree-Fock calculations. A simpler process to describe the Z-dependence of the broadening consists to assign the two splitting components to the "spin-up" and "spin-down" 2s electrons. Neglecting the change in wave functions with Z, the splitting energy δE is then expected to be proportional to S and to the binding energy B_{L1} of the 2s electron:

$$\delta E(Z) = \varepsilon S(Z) B_{L1}(Z) \quad (5)$$

For the trivalent core Sm^{3+} ions embedded in the metal crystal, $S = 2.5$ so that the yield ratio $I_1 \div I_2$ derived from (4) should be equal to 1.40. To determine the splitting coefficient ε, we refitted the Sm L_1-M_5 transition with two components. The width of the two Lorentzians was fixed at the value of 4.16 eV derived from the level widths given by Campbell and Papp and the intensity ratio at the above-mentioned value of 1.40. From the fit, a splitting δE = 2.54 ± 0.38 eV was obtained, which led to $\varepsilon = 1.31(20)\times10^{-4}$. The one- and two-components fits of the L_1-M_5 transition of Sm are depicted in Fig. 6. For clarity the tails of the L_3-$N_{4,5}$ line, the L_1-M_4 and L_3-O_1 lines as well as the N-satellite of the latter and the background were subtracted beforehand from the measured L_1-$M_{4,5}$ spectrum. Approximately equal chi-squares were found for the one- and two-components fits.

To probe the goodness of the splitting model, we have compared the fitted linewidths of the L_1-M_5 transitions of Ho and Yb with the FWHM widths of theoretical profiles obtained from the sum of two Lorentzians of equal width. The latter was derived from [5] whereas the energy difference and intensity ratio of the two Lorentzians were determined from (4) and (5), using for ε the value deduced from the two-component fit of Sm. Energy splittings of 2.47(37) eV and 0.69(10) eV, and intensity ratios of 1.5 and 3.0 were found for Ho ($S = 2$)

and Yb (S = ½). The resulting FWHM widths of the corresponding theoretical profiles were found to be 7.09 ± 0.39 eV and 6.86 ± 0.09 eV, respectively, both results in fair agreement with the L_1-M_5 linewidths presented in Table II. Applying the same method to the other rare-earth elements and subtracting from the obtained theoretical linewidths the $M_{4,5}$ level widths quoted in [5], we were able to determine a new set of L_1 widths for the lanthanides region. The proposed new values are presented in Fig. 5 (dotted line).

As shown in Table III, our experimental L_1 level widths are in general smaller than the corresponding theoretical predictions. The reason for the discrepancy resides mainly in the theoretical Coster-Kronig yields which are in most cases overestimated by the calculations. For the Sm and Ho, an opposite trend is observed but this is due to the above-mentioned broadening of the L_1 level in rare-earth elements which is not considered in the calculations. Finally, subtracting the L_1 widths obtained in the present work from the observed linewidths of the L_1-N_3 transition of Sm and L_1-M_2 and L_1-N_3 transitions of Ho reported in the preceding section, values of 2.22(52) eV and 4.39(38) eV are found for the N_3 level widths of Sm and Ho and of 7.61(40) eV for the M_2 level width of Ho. The corresponding widths quoted by Campbell and Papp are 2.2(5) eV, 2.95(50) eV and 6.3(7) eV. A good agreement is thus observed for the N_3 level of Sm whereas differences of about 1.3 eV are found for both the N_3 and M_2 level widths of Ho.

V. CONCLUDING REMARKS

High-resolution measurements of the L_1-$M_{4,5}$ fluorescence x-ray lines of Bi, Hg, Pt, W, Yb, Ho and Sm were performed. Despite the poor intensity of the dipole-forbidden transitions precise energies and linewidths were obtained. A comparison of the present experimental energies with differences between the binding energies of atomic levels listed by Bearden and Burr has shown that the latter binding energies have to be considered with precaution, deviations of several eV, i.e. larger than the quoted uncertainties, being frequently observed. Assuming for the $M_{4,5}$ level widths the values reported recently by Campbell and Papp, the L_1 level widths of the seven elements could be determined with a precision of 4%-10%. Whereas an excellent agreement with Campbell and Papp's data was observed for the five heaviest elements, an intriguing discrepancy was found for Ho and Sm. The observed deviations were explained by a splitting effect of the L_1 subshell resulting from the coupling of the 2s electron spin in the initial excited state with the total spin of the open 4f level. Based on this splitting picture, adjustements of the L_1 level widths recommended by Campbell and Papp were proposed for the lanthanides region. As in their work Campbell and Papp have determined the M_2 and M_3 level widths from XES measurements of the L_1-$M_{2,3}$ transitions, assuming their recommended L_1 level widths, the $M_{2,3}$ level widths they proposed, for the rare-earth might be overestimated. The same remark holds for the $N_{2,3}$ levels. Finally, in our opinion, a similar splitting effect should affect the width of the M_1 subshell of lanthanides.

This point could be clarified by high-resolution measurements of the L_3-M_1 transitions of rare-earths. Such measurements are in progress at out laboratory.

ACKNOWLEDGMENT

This work was partly supported by the Swiss National Science Foundation.

---

[1] O. Keski-Rahkonen and M. O. Krause, At. Data Nucl. Data Tables **14**, 139 (1974).

[2] S. I. Salem and P. L. Lee, At. Data Nucl. Data Tables **18**, 234 (1976).

[3] M. O. Krause and J. H. Oliver, J. Phys. Chem. Ref. Data **8**, 329 (1979).

[4] J. L. Campbell and T. Papp, X-ray Spectrom. **24**, 307 (1995).

[5] J. L. Campbell and T. Papp, At. Data Nucl. Data Tables **77**, 1 (2001).

[6] P.-A. Raboud, J.-Cl. Dousse, J. Hoszowska, I. Savoy, Phys. Rev. A **61**, 12507 (2000).

[7] J. Hoszowska, J.-Cl. Dousse, and Ch. Rhême, Phys. Rev. A **50**, 123 (1994).

[8] R. Stötzel, U. Werner, M. Sarkar, and W. Jitschin, J. Phys. B **25**, 2295 (1992).

[9] T. Papp, J. L. Campbell, and S. Raman, Phys. Rev. A **58**, 3537 (1998).

[10] U. Werner and W. Jitschin, Phys. Rev. A **38**, 4009 (1988).

[11] S. T. Perkins, D. E. Cullen, M.-H. Chen, J. H. Hubbell. J. Rathkopf, and J. H. Scofield, *Tables and Graphs of Atomic Subshell Relaxation Data* derived from the LLNL Evaluated Atomic Data Library, Lawrence Livermore National Laboratory report UCRL-50400, Vol. **30**, (1991).

[12] J. N. Cooper, Phys. Rev. **65**, 155 (1944).

[13] S. P. Kowalczyk, L. Ley, R. L. Martin, F. R. McFeely, and D. A. Shirley, Faraday Discuss. Chem. Soc. **60**, 7 (1975).

[14] B. Perny *et al*., Nucl. Instrum. Methods A **267**, 120 (1988).

[15] W. Beer, P. F. A. Goudsmit, and L. Knecht, Nucl. Instrum. Methods Phys. Res. A **219**, 322 (1984).

[16] W. Schwitz, Nucl. Instrum. Methods **154**, 95 (1978).

[17] R. C. Sharma *et al*., Nucl. Instrum. Methods **130**, 305 (1975).

[18] Ch. Herren and J.-Cl. Dousse, Phys. Rev. A **53**, 717 (1975).

[19] E. G. Kessler, Jr., R. D. Deslattes, D. Girard, W. Schwitz, L. Jacobs, and O. Renner, Phys. Rev. A **26**, 2696 (1982).

[20] J. Hoszowska, J.-Cl. Dousse, J. Kern and Ch. Rhême, Nucl. Instrum. Methods Phys. Res. A **376**, 129 (1996).

[21] J. A. Bearden, Rev. Mod. Phys. **39**, 78 (1967).

[22] F. James and M. Roos, Comput. Phys. Comm. **10**, 343 (1975).

[23] J. H. Scofield, At. Data Nucl. Data Tables **14**, 121 (1974).

[24] S. I. Salem, C. W. Schultz, B. A. Rabbani, and R. T. Tsutsui, Phys. Rev. Lett.**27**, 477 (1971).

[25] S. I. Salem and B. L. Scott, Phys. Rev. A **9**, 690 (1974).

[26] F. Parente, M. H. Chen, B. Crasemann and H. Mark, At. Data Nucl. Data Tables **26**, 383 (1981).

[27] W. Uchai, C. W. Nestor, Jr., S. Raman, and H. Mark, At. Data Nucl. Data Tables **34**, 201 (1986).

[28] M. H. Chen, B. Crasemann, and H. Mark, At. Data Nucl. Data Tables **24**, 13 (1979).

[29] E. G. Kessler, Jr., R. D. Deslattes, and A. Henins, Phys. Rev. A **19**, 215 (1979).

[30] E. R. Cohen and B. N. Taylor, J. Phys. Chem. Ref. Data **2**, 663 (1973).

[31] J. A. Bearden, A. F. Burr, Rev. Mod. Phys. **39**, 125 (1967).

[32] E. Storm and H. Israel, At. Data Nucl. Data Tables **7**, 565 (1970).

[33] G. Williams, http://xray.uu.se/hypertext /EbindEnergies.html.

[34] J. C. Fuggle, N. Mårtensson, J. Electron Spectrosc. Relat. Phenom. **21**, 275 (1980).

[35] S. Svensson *et al.*, J. Electron Spectrosc. Relat. Phenom. **9**, 51 (1976).

[36] B. D. Shrivastava, R. K. Jain, A. Mishra, and Devendra Singh, J. Phys. B **19**, 3839 (1986).

[37] E. J. McGuire, Phys. Rev. A **3**, 587 (1971).

[38] M. Ohno and R. E. LaVilla, Phys. Rev. B **39**, 8852 (1989).

[39] M. Ohno and R. E. LaVilla, Phys. Rev. A **45**, 4713 (1992).

[40] I. Arcon, A. Kodre, M. Štuhec, D. Glavic-Cindro, and W. Drube, Phys. Rev. A **51**, 147 (1995).

[41] O. Keski-Rahkonen, G. Materlik, B. Sonntag, and J. Tulkki, J. Phys. B: At. Mol. Phys. **L121** (1984).

[42] R. L. Cohen, G. K. Wertheim, A. Rosenwaig, and H. J. Guggenheim, Phys. Rev. B **5**, 1037 (1972).

Energy dependent KL double photoexcitation of Argon

P.-A. Raboud, M. Berset, J.-Cl. Dousse, Y.-P. Maillard, O. Mauron

Departement of Physics, University of Fribourg, Ch. du Musée 3, CH-1700 Fribourg, Switzerland

J. Hoszowska

European Synchrotron Radiation Facility (ESRF), F-38-043 Grenoble, France

M. Polasik

Faculty of Chemistry, Nicholas Copernicus University, 87-100 Torun, Poland

J. Rzadkiewicz

Soltan Institute for Nuclear Studies, 05-400 Otwock-Swierk, Poland

The fluorescence $K\alpha$ x-ray emission of argon induced by impact with monoenergetic photons was observed with a high-resolution reflecting type bent crystal spectrometer. The measurements were performed at the European Synchrotron Radiation Facility (ESRF) in Grenoble, France. X-ray beam energies in the range 3455 eV ≤ $\hbar\omega$ ≤ 6540 eV were used to investigate the *KL* double excitation from the threshold to saturation. The excitation probabilities were deduced from the satellite-to-diagram line yields ratios $\mathrm{I}(K\alpha L^{(1)}) : \mathrm{I}(K\alpha L^{(0)})$. Results were compared to theoretical predictions based on the model of Thomas and the one of Roy. From the comparison, parameters such as excitation onset energies, high-energy limit ionization probabilities and radius of the 2*p* orbital in ionic Ar were deduced. The satellite line shapes and their evolution with the excitation energy were analysed with the aid of MCDF calculations.

PACS number(s) : 32.30 Rj, 32.80 Fb, 32.70.-n, 34.50.Fa

I. INTRODUCTION

Due to atomic inner-shell electron correlations, the 1*s* photoionization of atoms may be accompanied by the ejection into the continuum of a second core-electron or by the promotion of the latter to an unfilled upper level. As a consequence photo-absorption spectra above the *K* edge are characterized by weak structures corresponding to shakeup single ionization and shakeoff double-ionization thresholds. Rare gases are especially suitable for investigation of these small contributions because their spectra do not exhibit EXAFS structures. In near-threshold photo-absorption measurements such *K*+*L* or *K*+*M* double excitation features were successfully in Ne, Ar and Kr [1-3].

An alternative method of studying these multielectron effects consists to observe the *K* fluorescence emission spectra. As a result of the multiple core-vacancy configuration characterizing the initial and final states, such

spectra evince indeed satellite structures whose intensity vary as a function of the excitation energy. This method was applied successfully to determine the evolution of the Cu $K\alpha L^{(1)}$ satellite line [4,5] (i.e. the $2p$-$1s$ transition with one additional spectator vacancy in the L-shell from threshold to saturation. More recently, the same technique was employed using the fluorescence valence $K\beta_2 M^{(1)}$ satellite transition from a solid Ge tar-get [6]. In the case of noble gases experimental results obtained by means of this method are scarce. For Ar some data have been published but they concern only the K+M double excitation. In this pioneering study [2] the $K\beta_{1,3}M^{(1,2)}$ satellite region was investigated at incident photon energies of 3199.2 eV, 3213.1 eV, 3245.9 eV and 3281.4 eV, i.e below and above the threshold energy for KM double photoexcitation.

In the present paper we report on high-resolution measurements of the $K\alpha_{1,2}L^{(1)}$ satellite x-ray emission of gaseous Ar bombarded by monochromatic photons with energies ranging between 3455 eV (onset energy for the double KL excitation) and 6540 eV (saturation limit). The satellite structure shape and the evolution of the latter as a function of the excitation energy were compared to theoretical profiles based on extensive multi-configuration Dirac-Fock (MCDF) calculations. From the measured $K\alpha_{1,2}L^{(1)}$: $K\alpha_{1,2}L^{(0)}$ satellite yield ratios corrected for those atomic rearrangement processes that modify the number of L spectator holes and occur prior to the K x-ray emission, the probabilities for producing via shake and two-step-one (TS1) processes the $K^{(1)}L^{(1)}$ double vacancy states were deduced. The variation as a function of the x-ray beam energy of the so-determined probabilities could be well reproduced by the model of Thomas [7] as well as by the model published recently by Roy *et al*. [8]. The high-energy limit probabilities obtained from the fits of the two models to our experimental data were compared to theoretical predictions based on the sudden approximation. A good agreement was observed. Other free fitting parameters entering the Thomas and Roy models such as the onset energies for the double $1s2p$ and $1s2s$ excitations and the L-shell radius of the Ar^{1+} ion were found to agree reasonably well with results of MCDF calculations.

II. EXPERIMENT

The measurements were performed at the European Synchrotron Radiation Facility (ESRF), Grenoble, France, with a high-resolution reflecting-type von Hamos curved crystal spectrometer. The latter was installed at the x-ray microscopy beamline ID21 downstream of the STXM microscope chamber to which it was connected through a ~180 cm long evacuated pipe. On the spectrometer side the pipe was closed with a 25 μm thick Kapton window in order to permit an access to the spectrometer chamber without degrading the high-vacuum in the beamline. The x-ray beam was monochromatized by a fixed exit Si(111) double-crystal mono-chromator having a resolving power of 10^{-4}, i.e. an energy resolution better than 1 eV over the entire energy domain of interest (3200 eV – 6500 eV). In order to minimize the contribution of high-energy photons to the

observed satellite yields, an efficient rejection of upper harmonics was needed. The latter was realized by a Si-based Ni coated mirror device. With this mirror, tilted by 8.2 mrad with respect to the beam direction, an harmonic rejection better than 10^{-3} and a transmission bigger than 70% could be achieved. Due to the weak intensity of the observed *L* satellite structures, 10^{11}-10^{12} incident photons/s were needed to obtain data of sufficient statistical quality. For this reason a beam size of 2 mm in diameter had to be used.

A detailed description of the von Hamos spectrometer can be found in [9]. The instrument consists mainly of an x-ray source defined by a rectangular slit, a cylindrically bent crystal and a position sensitive detector which are all enclosed in a stainless steel vacuum chamber. The 180-cm long × 62-cm wide × 24.5-cm chamber can be pumped down to 10^{-7} mbar by a turbomolecular pump. In the present experiment, the rectangular slit was made of two juxtaposed Ta pieces 0.3 mm thick and 10 mm high. The slit width was 0.2 mm. For diffraction of the x-rays a 5 cm wide and 10 cm high SiO_2 $(1\bar{1}0)$ crystal (spacing constant $2d$ = 8.5096 Å) was used. The crystal lamina was bent cylindrically to a radius of 25.4 cm. Reflected x rays were detected by a 50 μm thick CCD (Charge Coupled Device) position sensitive detector consisting of 1024×256 pixels with a pixel size of 27×27 μm. The 27.65 mm long and 6.9 mm high CCD was cooled down to –60 °C. The gaseous target consisted of a cylindrical cell filled up with 1 bar 99.999% pure argon. The cell was 10 mm in diameter with a 3.6 mg/cm^2-thick black Kapton wall. Black Kapton was chosen to protect the CCD detector from the visible light emitted by the irradiated argon. In order to minimize the absorption of the beam and the fluorescence x-rays in the gaseous target, the position of the latter was optimized using a 2-axes translation table. The beam intensity was monitored by measuring the $K\alpha + K\beta$ x-ray emission from the target with a 100 μm thick × 7 mm^2 Si photodiode. The latter was fixed on the top of the bent crystal support, perpendicularly to the target-crystal direction, viewing through the slit the same part of the target as the bent crystal.

The instrumental response of the spectrometer was determined from the measurement of the Ar $K\alpha_1 L^{(0)}$ diagram line excited by impact with 3206 eV photons for which only single *K*-shell ionization is energetically possible and consequently no broadening by unresolved *M*-satellites occurs. This narrow line could be well fitted with a single pure Lorentzian profile. From the fitted width (1.39 eV) and the transition width (0.79 eV) quoted in [10] for the K-L_3 transition, an instrumental broadening of 0.60 eV was deduced. The same measurement was employed for the energy calibration of the spectrometer using the formula (3) given in [9] and the Ar $K\alpha_1$ wavelength quoted by Bearden [11]. Since Bearden's values are listed in the Å* scale, the Ar $K\alpha_1$ wavelength was first corrected by the conversion factor 1.0000167 Å/Å* [12] and then converted to energy using the energy-wavelength product $V\lambda$=12398.520 eV Å [13], leading finally to an energy of 2957.8 eV.

The near-threshold variation of the Ar *KL* double excitation was investigated with 12 x-ray beam energies ranging from 3455 eV to

4000 eV. The absolute energy scale of the monochromator was adjusted by measuring with a photodiode the *K* absorption edge of Ar (3205.9 eV [14]). A crosscheck of the calibration was performed by measuring with the von Hamos spectrometer the line corresponding to the elastic scattering in the Ar target of the 3206 eV beam. No significant deviation was observed. In order to compare our experimental results with theoretical predictions based on the sudden approximation model which is valid only at the saturation limit, an additional measurement was performed at a higher energy (6540 eV). A new calibration of the monochromator was performed for this energy, using the *K* absorption edge of Mn (6539.0 eV[15]).

The von Hamos geometry permits at one position of the spectrometer components data acquisition over an energy bandwidth which is limited by the detector length. With the setup employed at ESRF, the bandwidth covered by the spectrometer was 69 eV so that the $K\alpha L^{(0)}$ diagram and $K\alpha L^{(1)}$ satellite lines could be measured within a single CCD length. This could have made the determination of the relative satellite yields independent from the beam intensity fluctuations. However, because different collecting times were chosen for the diagram and satellite lines, we did not take advantage of this autonormalization property. Different exposure times were chosen for the following reason. The charge left in a CCD pixel as a result of a photon impact is proportional to the deposited photon energy and a good x-ray event is characterized by a single pixel containing the whole specific energy. Thus, event recognition and selection proceeds by setting an energy window. In order to avoid multiple hit events, which are rejected by the energy window during the event sorting process, collecting times have to be chosen to minimize multiple hit events. For this reason, collecting times longer than 1 s could not be used at ESRF for the intense Ar $K\alpha L^{(0)}$ diagram line. On the other hand, the time needed by the CCD controller for reading a 1024 × 256 pixels frame is about 2.6 s so that more than 70% of the beam time is lost when exposure times of 1 s are chosen. In order to employ efficiently the allocated beam longer exposure times were thus chosen for the measurements of the much weaker satellite lines. Finally, for the above mentioned reasons, for each beam energy the measurements were performed in a sequence consisting of two short measurements with a longer measurement in between. In short measurements typically 200 images with an exposure time of 1 s per image were collected. An example of such a short measurement is given in Fig. 1. Depending on the beam intensity and the double excitation cross section, longer scans consisted of 350-2000 images, with a an

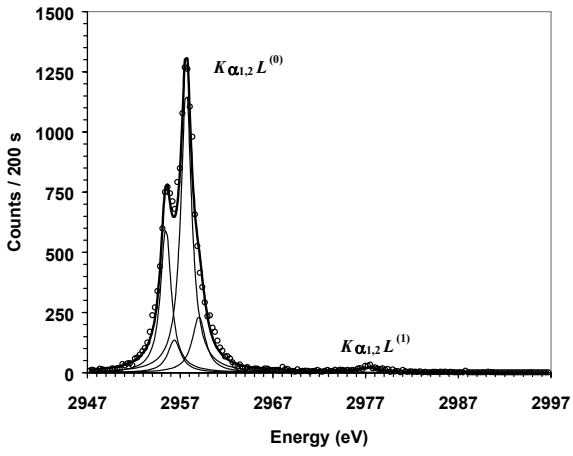

FIG. 1 High-resolution $K\alpha$ x-ray spectrum of Ar induced by impact with 3800 eV photons.

exposure time of 10 s per image. Short and long scans were corrected for the beam intensity fluctuations, using the corresponding monitor detector $K\alpha$+$K\beta$ yields. For each excitation energy, the intensity of the $K\alpha L^{(0)}$ diagram line was then computed from the average yield of the two short scans and the intensity of the $K\alpha L^{(1)}$ satellite from the yield of the associated longer measurement.

III. DATA ANALYSIS

The high-resolution x-ray spectra were analyzed by means of the least-squares-fitting computer program MINUIT [16] (CERN library), employing Lorentzian profiles to fit the diagram and satellite lines. Lorentzians were used because the convolution of the Lorentzian profile of the spectrometer response with the natural line shape of the x-ray transitions remains a Lorentzian.

The $K\alpha_1$ and $K\alpha_2$ diagram lines were fitted with two Lorentzians each, one for the main line, the second one for the unresolved *M*-satellite (see Fig. 1). The Lorentzian width of the two main lines were kept fixed at the value (1.39 eV) found from the fit of the satellite-free $K\alpha_1$ line measured with the 3206 x-ray beam whereas the yield ratios I[$K\alpha_2$]÷I[$K\alpha_1$] and I[$K\alpha_{1,2}M^{(1)}$]÷I[$K\alpha_{1,2}M^{(0)}$] were set, respectively, at 0.507 (MCDF prediction) and 0.229 (from Ref. [17]). The *L*-satellite structure was fitted with several Lorentzians whose positions, amplitudes, and widths were used as free-fitting parameters. Depending on the excitation energy, two or three Lorentzians were required to reproduce the observed satellite shapes. The relative yields $[X_{K\alpha 1,2L^{(1)}}]_i : X_{K\alpha 1,2L^{(0)}}$ of the three satellite components obtained from the fits are given in Table I as a function of the x-ray beam energy.

TABLE I Fitted relative intensities in (%) of the three satellite components.

	Satellite intensity		
	1st component	2nd component	3rd component
Beam energy	2977 eV	2974 eV	2968 eV
3455	0.00 ± 0.01		
3457	0.00 ± 0.01		
3500	0.05 ± 0.01		
3510	0.16 ± 0.02	0.05 ± 0.01	
3512	0.17 ± 0.02	0.06 ± 0.01	
3525	0.27 ± 0.03	0.08 ± 0.02	
3550	0.46 ± 0.03	0.12 ± 0.02	
3575	0.71 ± 0.04	0.14 ± 0.02	
3600	0.78 ± 0.04	0.16 ± 0.03	
3700	1.09 ± 0.04	0.19 ± 0.03	0.13 ± 0.02
3800	1.22 ± 0.05	0.22 ± 0.03	0.15 ± 0.02
4000	1.42 ± 0.05	0.31 ± 0.04	0.15 ± 0.02
6540	1.65 ± 0.13	0.56 ± 0.09	0.21 ± 0.09

IV. RESULTS AND DISCUSSION

A. Satellite line shape

As the *L* spectator vacancy can be located in 3 different subshells and because many couplings between the *K* and *L* holes in the initial state and the 2 *L* holes in the final state are possible, $K^{(1)}L^{(1)} \rightarrow L^{(2)}$ satellite transitions consist of many overlapping components that vary in energy and strength. As a consequence, the natural line shape of *L*-subshell satellite x-ray transitions is in general complex, showing asymmetries and fine structures that cannot be reproduced by single Gaussian, Lorentz or Voigt profiles. On the other hand, one would expect the overall line shape of the satellite transition to depend on the *L*-subshell in which the spectator hole is located. Similarly, one would expect that satellite transitions decaying two-core-vacancy states in Ar^{1+} (shakeup) differ in line shape from those

in Ar^{2+} (shakeoff). In other words, an evolution of the satellite line shape should be observed when varying the excitation energy from threshold to saturation.

To verify the above assumptions we have computed the theoretical profiles of the $K\alpha_{1,2}L^{(1)}$ satellites, employing MCDF calculations to determine the energies and transition probabilities of the different components pertaining to a particular satellite transition. The MCDF calculations were performed with the MSAL (modified special average level) [18] of the GRASP code [19]. The final results of the MCDF calculations are "stick" spectra consisting of many lines. To compare with measurements the lines were given a Lorentzian shape (FWHM = 1.4 eV). The transition profile was then constructed by computing the weighted sum of the Lorentz functions corresponding to different lines, the weighting factors being given by the transition probabilities. The calculations were performed for satellite transitions involving 2*p* and 2*s* spectator vacancies in Ar^{1+} and Ar^{2+}. To probe the goodness of the theoretical line shapes, the profile of the $K\alpha_{1,2}L^{(0)}$ diagram line was also simulated. The results are presented in Fig. 2. For the $1s^12p^54p^1 \rightarrow 1s^22p^44p^1$ (2*p* shakeup) and $1s^12p^5\varepsilon p \rightarrow 1s^22p^4\varepsilon p$ (2*p* shake-off) transitions 284 and 14 components, respectively, were considered whereas for the $1s^12s^12p^64s^1 \rightarrow 1s^22s^12p^54s^1$ (2*s* shakeup) and $1s^12s^12p^6\varepsilon s \rightarrow 1s^22s^12p^5\varepsilon s$ (2*s* shakeoff) transitions the number of summed components amounted to 19 and 6, respectively. As shown by Fig. 2, transitions decaying states populated by shakeup and shakeoff processes have practically the same shape, making thus

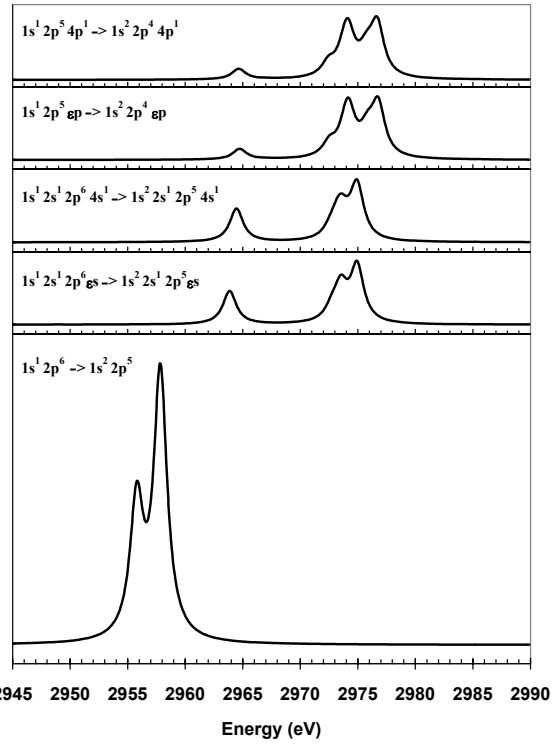

FIG. 2 Theoretical profiles based on MCDF calculations for the radiative decay in Ar of the 1*s* single-vacancy states ($K\alpha_{1,2}L^{(0)}$ diagram lines) and the 1*s*2*s* and 1*s*2*p* double vacancy states ($K\alpha_{1,2}L^{(1)}$ satellite lines).

impossible the distinction between shakeup and shakeoff excitation with the satellite technique employed in the present study. In contrast to that, the low energy component at about 2965 eV has a bigger relative intensity in transitions involving 2*s* spectator vacancy than those involving a 2*p* spectator vacancy. Thus this low energy component can be used as an experimental signature for distinguishing satellite transitions decaying $1s^{(1)}2s^{(1)}$ states from those originating from $1s^{(1)}2p^{(1)}$ states.

The measured $K\alpha_{1,2}L^{(1)}$ satellite spectra present a two-bump structure up to an excitation energy of 3600 eV whereas a third component had to be introduced in the analysis to fit properly the spectra taken at x-ray beam energies above 3600 eV. For illustration, the

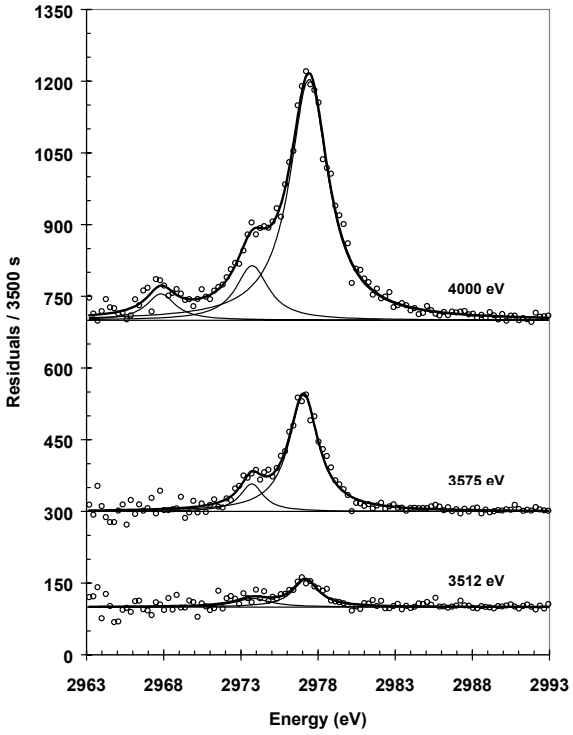

FIG. 3 Ar $K\alpha_{1,2}L^{(1)}$ satellite x-ray spectrum for three different excitation energies.

spectra measured at excitation energies of 3512 eV, 3575 eV and 4000 eV are presented in Fig. 3. The measurements confirm thus the MCDF calculations. Indeed, as predicted by the latter, the satellite structures measured above the threshold energy for 1*s*2*s* double electron excitation present a third component which is not visible at lower excitation energies and no particular feature in the line shape that could be related to shakeup excitations is seen in the spectra. However, it has to be noted that MCDF calculations fail in reproducing accurately the observed line shapes. For instance, the fitted centroid energies of the observed satellite components were found to be (2967.8 ± 0.5) eV, (2973.8 ± 0.2) eV and (2977.2 ± 0.1) eV. The corresponding energies predicted by the MCDF calculations are 2964 eV, 2974 eV and 2977 eV (see Fig. 2). A quite fair agreement is thus observed for the two high energy components but the low energy component is about 4 eV wrong. A more severe discrepancy between our results and the MCDF predictions resides in the yield ratio of the two high-energy components, the intensity of the 2974 eV bump being markedly overestimated by the calculations (see Figs. 2 and 3). Furthermore, the variation of the relative intensities of these two components as a function of the excitation energy (see Table I) could neither be explained in terms of the MCDF approach. We believe that these imperfections in the MCDF predictions arise from the use in the calculations of the *j-j* coupling scheme which is certainly not very adequate for Ar.

B. Energy dependence of the double excitation probability

The measured *L*-satellite yields reflect the distribution of the spectator holes at the moment of the *K* x-ray emission and not the initial distribution following the 1*s* photo-ionization which is the quantity of interest for the determination of the *L*-shell excitation probability. Processes such as *LMM* Auger and *L* radiative transitions occurring prior to the *K* x-ray emission can indeed modify the number of *L* spectator holes created just after the photon impact and named hereafter primary vacancies. Following the method described in details in the Appendix of Ref. [17] one finds for the primary vacancy yield ratio i_L:

$$i_L = \frac{x_L \omega_{K\alpha L^{(0)}} / \omega_{K\alpha L^{(1)}}}{1 - R_L (1 + x_L \omega_{K\alpha L^{(0)}} / \omega_{K\alpha L^{(1)}})} \quad (1)$$

where $x_L = X_{K\alpha L}{}^{(1)} : X_{K\alpha L}{}^{(0)}$ stands for the ratio of the measured satellite and diagram x-ray yields, $\omega_{K\alpha L}{}^{(n)}$ represents the partial K-shell fluorescence yield of the transition $K\alpha$ with n spectator holes in the L shell (n = 0,1) and R_L is a scaling factor describing the electron rearrangement. For Ar, $\omega_{K\alpha L}{}^{(0)} = 0.107$, $\omega_{K\alpha L}{}^{(1)} = 0.116$ and $R_L = 0.138$ [17]. The total probability for a single L-shell excitation is then given by:

$$P_L = \frac{8 i_L}{8 + i_L} \left(1 - \frac{i_L}{8 + i_L}\right)^7 \quad (2)$$

The probability P_L was calculated for each beam energy using relation (2). The obtained values are presented in Fig. 4 where they are compared to results of calculations based on the model of Thomas [7]. The point at 8810 eV was obtained from measurements using an x-ray tube for the target irradiation [17]. For comparison, it was added to the set of experimental data determined in the present study.

The probability for either exciting or ionizing an electron from a bound core-orbital as a result of an inner-shell vacancy production can be calculated using the so-called sudden approximation [20-23]. In this model the atomic excitation is treated separately from the initial vacancy production to which no reference is required except that the resulting change in the atomic potential due to the alteration in electron screening must be fast enough. The sudden approximation is thus valid if the adiabacity parameter $t_0 E_s / \hbar$ is much less than 1 [24]. Here E_s is the shake

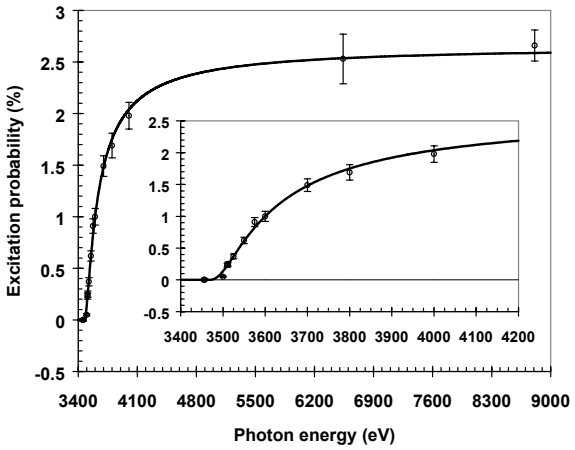

FIG. 4 Evolution of the Ar $K^{(1)}L^{(1)}$ double excitation probability as a function of the x-ray beam energy. The open circles represents the probabilities determined in the present study except the result at 8810 eV which was taken from [17]. The solid line shows the fit to the Thomas model [7] of the experimental probabilities. Only the total $2s + 2p$ excitation probability was considered.

energy and t_0 is the time during which the atomic potential changes and is therefore the time for the photoelectron to move a distance comparable to atomic dimensions. Conversely, the process will be adiabatic if $t_0 E_s / \hbar$ is much greater than 1. Using standard time-dependent quantum mechanics, Thomas has established an expression for understanding the crossover from the adiabatic to the sudden regime [7]. Within his description, the probability for creation of a second inner-shell hole via shake or TS1 (knockout of the second electron by departing photoelectron) process is given by:

$$P_{T\,hom\,as}(E_{ex}) = P_\infty \, exp\left(-\frac{m r^2 E_s^2}{2\hbar^2 E_{ex}}\right) \quad (3)$$

where P_∞ represents the probability at saturation, m the electron mass, r the above mentioned distance covered by the photoelectron during the time t_0 and E_{ex} the

energy needed for the excitation of the second core-electron. Replacing m and $\hbar$ by their values and expressing r in Angstroems and the energies in electronvolts, relation (3) can be expressed as:

$$P_{T\,hom\,as}(E) = P_\infty \, exp\left(-\frac{r^2 E_s^2}{15.32\left(E - E_{thr}\right)} \right) \quad (4)$$

Here E stands for the x-ray beam energy and E_{thr} is the threshold energy for double KL excitation in Ar. The fit of the function (4) to the experimental probabilities determined in the present study is represented by the solid line of Fig. 4. Free fitting parameters were P_∞, r and E_{thr} whereas E_s was kept fixed at 316.3 eV. This value was determined according to the (Z+1) potential approximation by computing the weighted average of the L-subshells binding energies of K (Z=19) quoted in [14]. From the fit the following results were obtained: $P_\infty = (2.66 \pm 0.04)\,\%$, $r = (0.15 \pm 0.01)$ Å, and $E_{thr} = (3451 \pm 6)$ eV.

To distinguish 2s and 2p electron excitation, a new fit was performed, employing the following extension of formula (4):

$$P_{T\,hom\,as} = P_{\infty,2s} \, exp\left(-\frac{r_{2s}^2 E_{2s}^2}{15.32\left(E - E_{thr,2s}\right)} \right)\delta_{i,+1} + P_{\infty,2p} \, exp\left(-\frac{r_{2p}^2 E_{2p}^2}{15.32\left(E - E_{thr,2p}\right)} \right)\delta_{j,+1} \quad (5)$$

where $\delta_{i,+1}$ and $\delta_{j,+1}$ are Kronecker symbols with i = sign of $(E - E_{thr,2s})$ and j = sign of $(E - E_{thr,2p})$. The shake energies E_{2s} and E_{2p} were set to values of 378.6 eV (binding energy of the L_1-subshell of K from [14]) and 295.5 eV (weighted average of the binding energies of the $L_{2,3}$-subshells of K from [14]), respectively. Other parameters were let free in the fit except r_{2s} which was fixed at the value of $1.10 \cdot r_{2p}$ according to Ref. [25]. Following results were found: $P_{\infty,2s} = (0.45 \pm 0.01)\,\%$, $P_{\infty,2p} = (2.19 \pm 0.04)\,\%$, $r_{2p} = (0.14 \pm 0.01)$ Å, $E_{thr,2s} = (3544 \pm 6)$ eV, $E_{thr,2p} = (3462 \pm 6)$ eV. The theoretical probabilities calculated from (5) with the above values for the free parameters are plotted in Fig. 5. From the examination of Fig. 4 and Fig. 5, one sees that the model of Thomas, using three or five free fitting parameters, reproduces quite well the

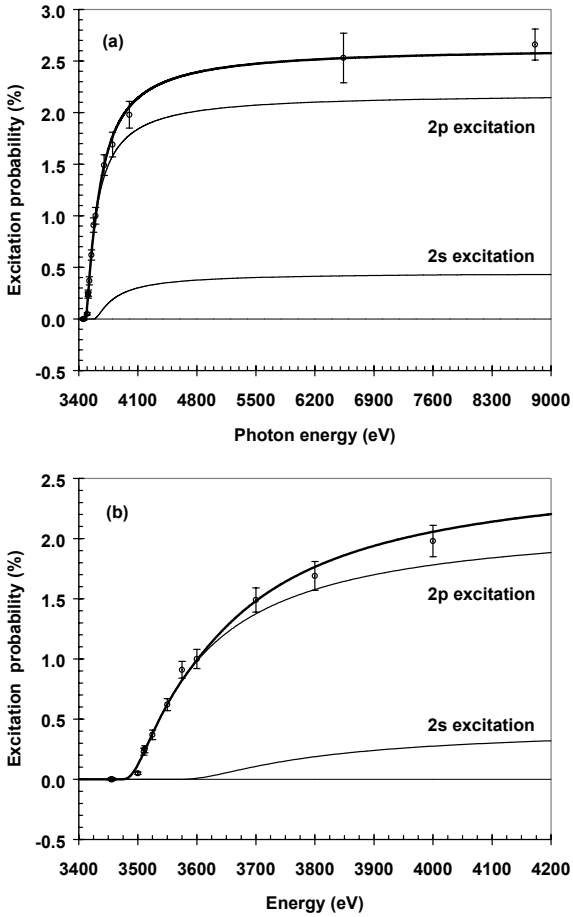

FIG. 5 (a) Same as Fig. 4 but separate 2p and 2s excitations were considered in the Thomas model. (b) Blow-up of the threshold energy region.

experimental probabilities determined in the present work and the one quoted in Ref. [17].

According to Krause [26], the breakdown point of the sudden approximation should occur at

$$\varepsilon = (E_{ph} - B_K - E_s) / E_s \quad (6)$$

where the numerator represents the excess energy of the incident photon over the ionization energy of the *K*-shell electron (B_K) plus the ionization energy of the shaken electron (E_s) which refers to an ion with a hole in the *K*-shell. Using Krause's recipe, one finds that for the double *KL* excitation of Ar, the sudden approximation should be valid above 6456 eV for 2*p* electrons and 6685 eV for 2*s* electrons. In [17], the target fluorescence was produced with the bremsstrahlung of an x-ray tube. The average bremsstrahlung energy was determined to be 8810 eV, an energy at which the sudden approximation should apply. The values obtained from the model of Thomas for P_∞ can thus be compared to the shake probability of $(2.66 \pm 0.18)\,\%$ reported in [17]. An excellent agreement is observed since results of $(2.66 \pm 0.04)\,\%$ and $(2.64 \pm 0.04)\,\%$ were obtained from 3- and 5-parameters fits, respectively. As mentioned in the introduction, available experimental information concerning *L*-shell shake in Ar is scarce. The single other experimental data found in the literature was obtained from photoelectron satellite measurements [27]. A value of $(2.5 \pm 0.8)\,\%$ is quoted, which is also consistent with our results. Several theoretical shake predictions based on the sudden approximation are available. Depending on the choice of the single-electron wave functions the results vary somewhat but in general they underestimate the experimental values. For the $2s/2p$ orbitals of Ar, results of 0.30%/1.59% [24], 0.31%/1.58% [28], 0.30%/1.75% [17] and 0.48%/2.55% [23] were published. The values quoted by Åberg [23] are larger than other theoretical predictions because the forbidden transitions to already occupied orbitals were not excluded in his calculations. Other calculations employing multihole configuration for the final ionic state [29] lead to values of 0.36%/2.13% which are closer to our results ($P_{\infty,2s} / P_{\infty,2p} = 0.45\%/2.19\%$).

Regarding the threshold energies, a result of (3451 ± 6) eV was derived from the 3-parameters fit. This value should correspond to the onset for 2*p* electron excitation and can thus be compared to the 2*p* threshold energy deduced from the 5-paremeters fit. As a value of (3462 ± 6) eV was found from the second fit, the two results are consistent within the quoted uncertainties. The onset energies for a double KL_i ionization (shakeoff) can be derived by adding the L_i-subshell binding energy of ionic Ar^{1+} to the *K*-shell binding energy of neutral Ar (3205.9 eV). Similarly, threshold energies for shakeup excitation can be deduced from differences in the binding energies of the Ar^{1+} ion in the electron configurations $1s^1 2s^2 2p^6 3s^2 3p^6$ and $1s^1 2s^2 2p^5 3s^2 3p^6 4p^1$, respectively $1s^1 2s^1 2p^6 3s^2 3p^6 4s^1$, and by adding the obtained values to 3205.9 eV. MCDF calculations were thus performed to determine the above binding energies. As precise absolute energies are difficult to carry out with MCDF calculations, the latter were anchored of neutral Ar and K to the values quoted in

[14]. From these adjusted MCDF calculations, the following onset energies were obtained:

$E_{thr}^{MCDF}(2p \text{ shakeoff}) = 3479.7 \text{ eV}$

$E_{thr}^{MCDF}(2s \text{ shakeoff}) = 3540.6 \text{ eV}$

$E_{thr}^{MCDF}(2p \text{ shakeup}) = 3468.4 \text{ eV}$

$E_{thr}^{MCDF}(2s \text{ shakeup}) = 3530.6 \text{ eV}$

Our experimental method does not permit to distinguish shakeup and shakeoff excitation. The experimentally determined onset energies can be compared, however, to the MCDF prediction concerning shakeup since the latter are expected to occur at lower excitation energies. As one can see, a more or less satisfactory agreement is observed (3462(6) eV versus 3468.4 eV for 2*p* and 3455(6) eV versus 3530.6 eV for 2*s*).

For the distance *r*, the third free fitting parameter, consistent values of 0.15(1) Å and 0.14(1) Å were found from the two fits. To better understand the meaning of *r*, MCDF calculations of the Ar 2*p* orbital radius were performed. The following results were obtained (r_{max} is the radius for which the squared 2*p* wavefunction peaks):

$< r_{2p} >(\text{neutral Ar}) = 0.198 \text{ Å}$

$< r_{2p} >(1s^1 \text{ Ar}^{1+}) = 0.185 \text{ Å}$

$r_{max,2p}(\text{neutral Ar}) = 0.149 \text{ Å}$

$r_{max,2p}(1s^1 \text{ Ar}^{1+}) = 0.144 \text{ Å}$

Although no precise definition is given for the distance *r* in the paper of Thomas [7], it is interesting to note that the average experimental value of 0.145(7) Å is very close to the radius r_{max} of the 2*p* orbital in the ionic Ar^{1+} and about 25% smaller than the average radius $< r_{2p} >$.

Another simple generic model permitting to calculate the probability of multiple electron excitation from threshold to saturation was published very recently by Roy *et al*. [8]. In this model the high-energy limit of the probability is calculated in the sudden approximation approach using Slater orbitals. At lower excitation energies, the calculations are based on a simple model form of the perturbing potential. The probability of exciting a spectator electron with a photon of energy $\hbar\omega$ is then given by (after correction of two printing mistakes appearing in the formula (18) quoted in [8]):

$$P(E) = P_\infty \frac{2^{2n}(n-1)!(n+1)!}{\pi(2n-1)!} \times \int_1^{\frac{E_p}{E_b}} \frac{(X-1)^{1/2}}{X^{n+2}\left(1+\left(\frac{n-1}{2}\right)^2 \frac{E_b}{E_p} X^2\right)} dX \quad (7)$$

where E_p is the kinetic energy of the photoelectron, E_b the binding energy of the shaken electron, *n* the principal quantum number of the shaken electron shell, and *X* a dimensionless parameter defined by $X := 1 + \hbar\omega / E_b$. Applying relation (7) to the case of the double *KL* excitation leads to

$$P(E) = P_\infty \frac{2^4}{\pi} \int_1^{\frac{E-B_K}{B_L}} \frac{(X-1)^{1/2}}{X^4\left(1+\frac{1}{4}\frac{B_L}{E-B_K} X^2\right)} dX \quad (8)$$

Using P_∞ and B_L as free fitting parameters, we tried to fit our data with relation (8). As for the Thomas model, the fitted function was found to reproduce well the experimental probabilities (see Fig. 6). The values returned

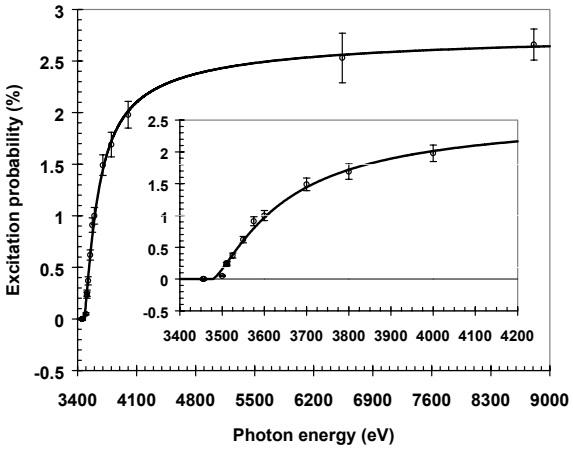

FIG. 6 Same as Fig. 4 but the solid line represents in this case the fit of the data to the model of Roy *et al.* [8].

by the fit for P_∞ and B_L are $(2.79 \pm 0.04)\%$ and (270.9 ± 2.5) eV, respectively. One sees that high-energy limit probability P_∞ is slightly overestimated by the new model but only by about 5 %. The value obtained for B_L agrees also rather well with the binding energies of the L_2 and L_3 subshells given by the adjusted MCDF calculations. The latter predict indeed energies of 274.7 eV and 283.0 eV for the binding energies of the $2p_{1/2}$ (J=0) and $2p_{1/2}$ (J=1) levels of the $1s^1$ Ar^{1+} ion, and 273.8 eV and 272.3 eV for the $2p_{3/2}$ (J=1) and $2p_{3/2}$ (J=2) levels. In the model of Roy, the distance r moved by the photoelectron during the perturbation is represented in formula (7) by the term (n-1) occurring in the denominator of the integral. According to the authors the term (n-1) is related to the parameter r_{max} discussed previously. If the expectation value $<r>$ is chosen instead of r_{max}, (n-1) has to be replaced in (7) by (n+1/2). We tried thus to fit also our data with the modified $(n-1 \rightarrow n+1/2)$ formula (7). A poor agreement was observed, indicating therefore that, as in the model of Thomas, the best results are obtained when the radius r_{max} of the excited orbital is chosen for the distance r.

ACKNOWLEDGMENT

This work was supported by the European Synchrotron Radiation Facility and the Swiss National Science Foundation. The authors would like thank Dr. J. Susini and his collaborators of ID21 for their support during the experiment.

[1] J. M. Esteva, B. Gauthe, P. Dhez, and R. C. Karnatak, J. Phys. B **16**, L263 (1983).

[2] R. D. Deslattes, R. E. LaVilla, P. L. Cowan, and A. Henins, Phys. Rev. A **27**, 923 (1983).

[3] S. J. Schaphorst, *et al.*, Phys. Rev. A **47**, 1953 (1993).

[4] M. Deutsch, O. Gang, K. Hämäläinen, and C. C. Kao, Phys. Rev. Lett. **76**, 2424 (1996).

[5] M. Fritsch, C. C. Kao, K. Hämäläinen, E. Förster, and M. Deutsch, Phys. Rev. A **57**, 1686 (1998).

[6] C. Sternemann, A. Karpolat, M. H. Krisch, and W. Schülke, Phys. Rev. A **61**, 020501 (2000).

[7] T. D. Thomas, Phys. Rev. Lett. **52**, 417 (1984).

[8] M. Roy, J. D. Lindsay, S. Louch, and S. J. Gurman, J. Synchrotron Rad. **8**, 1103 (2001).

[9] J. Hoszowska, J.-Cl. Dousse, J. Kern, and Ch. Rhême, Nucl. Instrum. Methods Phys. Res. A **376**, 129 (1996).

[10] J. L. Campbell and T. Papp, At. Data Nucl. Data Tables **77**, 1 (2001).

[11] J. A. Bearden, Rev. Mod. Phys. **39**, 78 (1967).

[12] E. G. Kessler, Jr., R. D. Deslattes, and A. Henins, Phys. Rev. A **19**, 215 (1979).

[13] E. R. Cohen, and B. N. Taylor, J. Phys. Chem. Ref. Data **2**, 663 (1973).

[14] M. Cardona and L. Ley, Eds., *Photoemission in Solids I* : Springer-Verlag, Berlin, (1978).

[15] F. B. Larkins, At. Data Nucl. Data Tables **20**, 313 (1977).

[16] F. James, and M. Roos, Comput. Phys. Commun. **10**, 343 (1975).

[17] J.-Cl. Dousse, and J. Hoszowska, Phys. Rev. A **56**, 4517 (1997).

[18] M. Polasik, Phys. Rev. A **40**, 4361 (1989).

[19] I. P. Grant *et al*., Comput. Phys. Commun. **21**, 207 (1980).

[20] F. Bloch, Phys. Rev. **48**, 187 (1935).

[21] L. G. Parrat, Rev. Mod. Phys. **31**, 616 (1959).

[22] T. Åberg, Phys. Rev. **156**, 35 (1967).

[23] T. A. Carlson and C. W. Nestor, Jr., Phys. Rev. A **8**, 2887 (1973).

[24] T. A. Carlson and M. O. Krause, Phys. Rev. **140**, A 1057 (1965).

[25] J. P. Desclaux, At. Data Nucl. Data Tables **12**, 312 (1973).

[26] M. O. Krause, J. Phys. (Paris) Colloq. Suppl. 10 **32**, C4-67 (1971).

[27] M. O. Krause, T. A. Carlson, and R. D. Dismukes, Phys. Rev. **170**, 37 (1968).

[28] T. A. Mukoyama and K. Tamiguchi, Phys. Rev. A **36**, 693 (1987).

[29] K. G. Dyall, J. Phys. B **16**, 3137 (1983).

List of publications

Refereed articles

L_1 to N_5 atomic level widths of thorium and uranium as inferred from measurements of L and M x-ray spectra.

P.-A. Raboud, J.-Cl. Dousse, J. Hoszowska, I. Savoy

Published in Physical Review A 61, 012507 (2000)

L_1 atomic level width of elements $62 \leq Z \leq 83$.

P.-A. Raboud, M. Berset, J.-Cl. Dousse, Y.-P. Maillard

Accepted for publication in Physical Review A

Energy dependent KL double photoexcitation of Argon.

P.-A. Raboud, M. Berset, J.-Cl. Dousse, J. Hoszowska, Y.-P. Maillard, O. Mauron, M. Polasik, J. Rzadkiewicz

Submitted to Physical Review A

L-Shell ionization in near-central collisions of heavy ions with low-Z atoms.

M. Kavcic, M. Budnar, A. Mühleisen, P. Pelicon, Z. Smit, M. Zitnik, D. Castella, D. Corminboeuf, J.-Cl. Dousse, J. Hoszowska, P.-A. Raboud, K Tökési

Published in Physical Review A 61, 052711 (2000)

Influence of the chemical environment on the Si KL x-ray satellite spectra of transition metal silicides bombarded by 43 MeV neon ions.

J. Hoszowska, J.-Cl. Dousse, D. Castella, D. Corminboeuf, J. Kern, Y.-P. Maillard, P.-A. Raboud

Published in Journal of Physics B: Atomic, Molecular and Optical Physics 33, 3165 (2000)

Trapping of Xenon Induced in Polymeric Films by UV and X-ray Irradiation.

D. Castella, D. Corminboeuf, J.-Cl. Dousse, J. Hoszowska, Y.-P. Maillard, P.-A. Raboud

Published in Macromolecules, 33, 8583 (2000)

High-resolution measurements of Th and U L-x-rays induced by O ions.

M. Pajek, D. Banas, D. Castella, D. Corminboeuf, J.-Cl. Dousse, Y.-P. Maillard, O. Mauron, P.-A. Raboud, D. Chmielewska, I. Fijal, M. Jaskola, A. Korman, T. Ludziejeski, J. Rzadkiewicz, Z. Sujkowski, M. Polasik, J. Hoszowska and T. Mukoyama

Physica Scripta T 92, 382 (2001)

Conference abstracts

Reduced velocity dependence of the L shell ionization by heavy ions in near central collisions with low Z atoms.

M. Kavcic, M. Budnar, A. Mülheisen, Z. Smit, D. Castella, J.-Cl. Dousse, J. Hoszowska, P.-A. Raboud

6th European Conference on Atomic and Molecular Physics, Siena, Italy, 14-18 July 1998, Europhys. Conf. Abstr. 22D (1998) I-68

Influence of the Chemical State on the Si KL x-ray Satellite Spectra of Transition Metal Silicides bombarded by 43 MeV Ne^{3+} ions.

J. Hoszowska, D. Castella, J.-Cl. Dousse, Y.-P. Maillard and P.-A. Raboud

Fifteenth International Conference on the Applications of Accelerators in Research & Industry (Denton, 1998), book of abstracts, p. 82

The M x-ray emission spectrum of thorium and uranium.

P.-A. Raboud, J-Cl. Dousse

18th International Conference on X-ray and Inner-Shell Processes, Chicago, Illinois , USA, 23-27 August 1999, book of abstracts p.186

L-Shell ionization in collision of heavy ions with low Z atoms.

M. Kavcic, M. Budnar, A. Mühleisen, P. Pelicon, Z. Smit, M. Zitnik, D. Castella, J.-Cl. Dousse, J. Hoszowska, P.-A. Raboud, K Tökési

18th International Conference on X-ray and Inner-Shell Processes, Chicago, Illinois, USA, 23-27 August 1999, book of abstracts p.141

High-resolution measurements of the L and M x-ray emission spectra of several heavy elements.

J.-Cl. Dousse, J. Hoszowska, Y.-P. Maillard and P.-A. Raboud

Sixteenth International Conference on the Applications of Accelerators in Research & Industry Denton, 2000, book of abstracts p.92

Trapping of rare gases induced in polymeric substrates by x-ray and uv irradiation.

J.-Cl. Dousse, D. Castella, D. Corminboeuf, J. Hoszowska, Y.-P. Maillard and P.-A. Raboud

European Conference on Energy Dispersive X-ray Spectrometry, EDXRS-2000, Krakov 2000, book of abstracts p. 56

High-resolution measurements of Th and U L-x-rays induced by O ions.
M. Pajek, D. Banas, D. Castella, D. Corminboeuf, J.-Cl. Dousse, Y.-P. Maillard, P.-A. Raboud, D. Chmielewska, I. Fijal, M. Jaskola, A. Korman, T. Ludziejeski, J. Rzadkiewicz, Z. Sujkowski, M. Polasik and J. Hoszowska
Physics of Highly Charged Ions HCI 2000, Berkeley 2000,book of abstracts

High-resolution study of thorium and uranium L x-ray spectra induced by impact with fast oxygen ions.
J.-Cl. Dousse, D. Banas, D. Castella, D. Chmielewska, D. Corminboeuf, I. Fijal, J. Hoszowska, M. Jaskola, A. Korman, T. Ludziejewski, Y.-P. Maillard, O. Mauron, M. Pajek, M. Polasik, P.-A. Raboud, J. Rzadkiewicz, and Z. Sujkowski
7th EPS Conf. on At. Mol. Phys. (Berlin, 2001), Europhys. Conf. Abs. 25 B (2001) 47

High-resolution study of L- and M-x-ray satellites excited in collisions of 360-MeV oxygen ions with heavy atoms
D. Banas, M. Berset, D. Chmielewska, D. Czarnota, J.-Cl. Dousse, J. Hoszowska, Y.-P. Maillard, O. Mauron, T. Mukoyama, M. Pajek, M. Polasik, P.-A. Raboud, J. Rzadkiewicz, and Z. Sujkowski
XXII International Conference on Photonic, Electronic and Atomic Collisions ICPEAC 2001 (Santa Fe, 2001), book of abstr.

Non-refereed papers and reports

Reduced velocity of the L shell ionization by heavy ions in near central collisions with low Z atoms.
M. Budnar, D. Castella, J.-Cl. Dousse, J. Hoszowska, M. Kavcic, J. Kern, A. Mülheisen, P.-A. Raboud, Z. Smit
PSI Annuel Report 1997 / Annex 1: Nuclear and Particle Physics, Muons in Solid State Physics and Chemistry, p. 95

Energies and linewidths of photoinduced M x rays of uranium.
P.-A. Raboud, J.-Cl. Dousse
20 Arbeitsbericht, Arbeitsgruppe Energiereiche Atomare Stösse, Gesellschaft für Schwerionenforschung (GSI),Darmstadt, April 1999, p. 70

M-(SUB) Shell Ionization in Collisions of Carbon Ions with Palladium.
J. Rzadkiewicz, D. Chmielewska, T. Ludziejewski, Z. Sujkowski, D. Castella, J.-Cl. Dousse, O. Mauron, Y.-P. Maillard, P.-A. Raboud, J. Hoszowska, M. Polasik, M. Pajek.
The Andrzej Soltan Institute for Nuclear Studies Annual Report 2000, p 43

High-resolution study of heavy-ion-induced Thorium and Uranium Lγx-ray spectra.

M. Pajek, D. Banas, D. Castella, D. Corminboeuf, J.-Cl. Dousse, J. Hoszowska, Y.-P. Maillard, P.-A. Raboud, D. Chmielewska, I. Fijal, M. Jaskola, A. Korman, T. Ludziejewski, J. Rzadkiewicz, Z. Sujkowski, M. Polasik and J. Hoszowska

PSI Scientific Report 2000 / Volume 1: Particles and Matter, p. 22

Curriculum vitae

Nom et Prénom	Raboud Pierre-Alexandre
Etat civil	Célibataire
Date de naissance	Le 7 août 1967
Lieu d'origine	Villarsiviriaux
Nationalité	Suisse

Formation

Scolarité obligatoire	1974-1980	Cercle scolaire d'Orsonnens
	1980-1983	Cycle d'orientation de Romont
	1983	Certificat d'études secondaires
Apprentissage	1983-1987	Université de Fribourg Institut de Chimie-Physique Mécanicien-électronicien
	1987	Certificat Fédéral de Capacité
Formation supérieure	1988-1992	Ecole Technique Supérieure de Fribourg Section d'électrotechnique
	1992	Diplôme d'ingénieur ETS Option Energie électrique Travail de diplôme: Etude et réalisation d'un programme permettant la simulation du comportement d'un moteur brushless de l'entreprise Portescap
Formation universitaire	1993-2001	Université de Fribourg Département de Physique Groupe de Physique Atomique
	1997	Diplôme de physicien Travail de diplôme: Evaluation d'un détecteur CCD et mesure de quelques transitions radiatives du thorium et du xénon
	1998-2001	Assistant diplômé

Remerciements

Je vous voudrais remercier ici toutes les personnes qui m'ont permis de réaliser cette thèse.

En premier lieu ma mère. Son soutien, ses encouragements et son dévouement à m'éviter tous les tracas domestiques de la vie m'ont permis d'accomplir mes études dans de bonnes conditions.

Un très grand merci va tout naturellement à mon directeur de thèse, le Prof. Dr. Jean-Claude Dousse, qui par ses compétences, son expérience, sa disponibilité a su me conseiller et me guider de manière judicieuse durant mon travail de thèse.

Merci à tous les membres de l'ancien groupe PAN et de l'actuel groupe FRAP pour l'ambiance de travail agréable et pour l'amitié qu'ils m'ont témoignée.

Un bon fonctionnement des instruments de mesure a permis la réalisation de ce travail. Je tiens donc à remercier également toute l'équipe de l'atelier de mécanique et les ingénieurs D. Corminboeuf et M. Berset qui ont travaillé sans compter pour rendre cela possible.

J'adresse aussi ma reconnaissance aux secrétaires, en particulier à Marie-Louise et Bernadette, qui effectuent un énorme travail dans l'ombre, mais combien nécessaire.

Je tiens encore à saluer la mémoire du Prof. Jean Kern, grand physicien et grand homme.

A tous ceux et toutes celles que j'aurais oublié de mentionner, je tiens à vous dire MERCI.